J. Fluid Mech. (1998), *vol.* 373, *pp.* 33–79. Printed in the United Kingdom

Mean-flow scaling of turbulent pipe flow

By MARK V. ZAGAROLA† AND ALEXANDER J. SMITS

Department of Mechanical and Aerospace Engineering, Princeton University, Princeton, NJ 08544, USA

(Received 11 November 1997 and in revised form 26 May 1998)

Measurements of the mean velocity profile and pressure drop were performed in a fully developed, smooth pipe flow for Reynolds numbers from 31×10^3 to 35×10^6. Analysis of the mean velocity profiles indicates two overlap regions: a power law for $60 < y^+ < 500$ or $y^+ < 0.15R^+$, the outer limit depending on whether the Kármán number R^+ is greater or less than 9×10^3; and a log law for $600 < y^+ < 0.07R^+$. The log law is only evident if the Reynolds number is greater than approximately 400×10^3 ($R^+ > 9 \times 10^3$). Von Kármán's constant was shown to be 0.436 which is consistent with the friction factor data and the mean velocity profiles for $600 < y^+ < 0.07R^+$, and the additive constant was shown to be 6.15 when the log law is expressed in inner scaling variables.

A new theory is developed to explain the scaling in both overlap regions. This theory requires a velocity scale for the outer region such that the ratio of the outer velocity scale to the inner velocity scale (the friction velocity) is a function of Reynolds number at low Reynolds numbers, and approaches a constant value at high Reynolds numbers. A reasonable candidate for the outer velocity scale is the velocity deficit in the pipe, $U_{CL} - \bar{U}$, which is a true outer velocity scale, in contrast to the friction velocity which is a velocity scale associated with the near-wall region which is 'impressed' on the outer region. The proposed velocity scale was used to normalize the velocity profiles in the outer region and was found to give significantly better agreement between different Reynolds numbers than the friction velocity.

The friction factor data at high Reynolds numbers were found to be significantly larger ($> 5\%$) than those predicted by Prandtl's relation. A new friction factor relation is proposed which is within $\pm 1.2\%$ of the data for Reynolds numbers between 10×10^3 and 35×10^6, and includes a term to account for the near-wall velocity profile.

1. Introduction

In the experiment presented here, a fully developed, smooth pipe flow was studied for Reynolds numbers from 31×10^3 to 35×10^6, where the Reynolds number Re is based on the average velocity $\bar{U}$ and the pipe diameter D. The highest Reynolds number investigated is an order of magnitude larger than the previous highest value achieved for mean-flow measurements in a smooth pipe (Nikuradse 1932; Dickinson 1975). The experiments were specifically undertaken to investigate the scaling of the mean velocity profile and friction factor. Since we come to conclusions that differ from the generally accepted scaling arguments, some historical background is necessary.

Most theoretical treatments for the scaling of pipe flow start by dividing the flow into a near-wall and core region. For each region, a length and velocity scale may be defined. The velocity scale in the near-wall region is typically taken to be the friction velocity u_τ given by

$$u_\tau = (\tau_w/\rho)^{1/2}, \tag{1}$$

† Current address: Creare Inc., Etna Road, PO Box 71, Hanover, NH 03755, USA.

where τ_w is the wall shear stress and ρ is the density. The length scale associated with the near-wall region is then the kinematic viscosity ν divided by the friction velocity, ν/u_τ. For the core region, the velocity scale is also typically taken to be the friction velocity, although this has long been a source of controversy (Zagarola & Smits 1997; George, Castillo & Knecht 1996), and the length scale is taken to be the radius R.

The ratio of length scales gives the Kármán number ($R^+ = Ru_\tau/\nu$) which for a pipe is a unique function of Reynolds number. As the Reynolds number changes, the shape of the mean velocity profile, or equivalently, the relative fraction of the flow occupied by the near-wall and core regions, also changes. If R^+ is large enough, it is usually assumed that the interaction between inner and outer regions vanishes because of the disparity of length scales, and consequently, independent similarity solutions may exist for each region.

As originally proposed by Prandtl (1933), the near-wall velocity profile depends on the distance from the wall, the wall shear stress and the fluid properties. That is,

$$U = f_0(y, \tau_w, \rho, \mu), \tag{2}$$

where f_0 expresses the functional relationship, y is the distance from the wall and μ is the dynamic viscosity. Dimensional analysis of (2) yields

$$U^+ = f_1(y^+), \tag{3}$$

where $U^+ = U/u_\tau$ and $y^+ = yu_\tau/\nu$. Equation (3) is known as the 'law-of-the-wall' and is valid only in the near-wall region. It can be shown from the Navier–Stokes equation that f_1 is linear near the wall, and we may expect that (3) is valid further from the wall than the linear region but not into the core region (i.e. (3) will hold for $0 < y^+ \quad R^+$).

In the core region, von Kármán (1930) argued that the wall acts to retard the local velocity below the maximum velocity in a way which is independent of the viscosity, but depends on the distance from the wall, the radius of the pipe, the wall shear stress and the density. That is, the velocity 'defect' should scale according to

$$U_{CL} - U = g_0(y, R, \tau_w, \rho), \tag{4}$$

where U_{CL} is the velocity at the centreline and g_0 expresses the functional relationship. Note that (4) does not depend on viscosity except through the wall shear stress. Dimensional analysis of (4) yields

$$U^+_{CL} - U^+ = g_1(\eta), \tag{5}$$

where $U^+_{CL} = U_{CL}/u_\tau$ and $\eta = y/R$. This functional relationship was first proposed by Stanton in 1911 (Schlichting 1987) and is known as the 'defect-law'. Equation (5) is valid only in the core region where viscosity is not important (i.e. (5) will hold for $0 \quad \eta < 1$). If f_1 and g_1 are independent of Reynolds number, complete similarity exists in each region; otherwise, incomplete similarity exists.

Millikan (1938) proposed that at large enough Reynolds numbers there may be a region of overlap where both the inner and outer similarity laws are simultaneously valid. This region exists for $\nu/u_\tau \quad y \quad R$ or $1 \quad y^+ \quad R^+$. By matching the velocity gradients found from (3) and (5), it follows that the form of the velocity profile in the overlap region must be logarithmic. When expressed using inner scaling variables the resulting equation is

$$U^+ = \frac{1}{\kappa}\ln y^+ + B, \tag{6}$$

where κ is known as von Kármán's constant and B is a constant that depends on the inner integration limit of the log law. In terms of outer scaling variables, the resulting equation is

$$U^+_{CL} - U^+ = -\frac{1}{\kappa}\ln\eta + B^*, \tag{7}$$

where B^* is a constant that depends on the outer integration limit of the log law. All three constants, κ, B and B^*, are empirical and have typical values of 0.41, 5.2 and 0.65, respectively, and the log region is believed to exist for $50\nu/u_\tau < y < 0.15R$. If the constants are independent of R^+, then complete similarity exists in the overlap region, and by virtue of the derivation of this overlap region, complete similarity also must exist in the inner and outer regions. The log law contants and the region of validity of the log law will be investigated in detail in §§7–10.

The friction factor λ for a pipe is defined as

$$\lambda = \frac{-(\mathrm{d}P/\mathrm{d}x)\,D}{\frac{1}{2}\rho\bar{U}^2}, \tag{8}$$

where $\mathrm{d}P/\mathrm{d}x$ is the mean streamwise pressure gradient which, for fully developed pipe flow, is constant and is related to the wall shear stress by $\tau_w = \frac{1}{2}R\,\mathrm{d}P/\mathrm{d}x$. Therefore,

$$\lambda = 8(u_\tau/\bar{U})^2. \tag{9}$$

The scaling of the mean velocity profile is related to the scaling of the friction factor by the definition of the average velocity. That is,

$$\left(\frac{8}{\lambda}\right)^{1/2} = \frac{\bar{U}}{u_\tau} = 2\int_0^1 U^+\left(1-\frac{y^+}{R^+}\right)\mathrm{d}\,\frac{y^+}{R^+}. \tag{10}$$

If the scaling of the mean velocity profile is known, then the scaling of the friction factor is also known.

Prandtl proposed a friction factor relationship based on complete similarity of the mean velocity profile (see Durand 1943). Prandtl integrated the log law (equation (6)) from the wall to the centreline to obtain

$$\left(\frac{8}{\lambda}\right)^{1/2} = \frac{1}{\kappa}\ln\left(Re\left(\frac{\lambda}{32}\right)^{1/2}\right) + B - \frac{3}{2\kappa}. \tag{11}$$

Prandtl rearranged this equation and adjusted the constants based on Nikuradse's (1932) friction factor data to obtain

$$\frac{1}{\lambda^{1/2}} = 2.0\log\left(Re\,\lambda^{1/2}\right) - 0.8. \tag{12}$$

This expression is known as *Prandtl's universal law of friction for smooth pipes* which Schlichting (1987) believes 'may be extrapolated to arbitrarily large Reynolds numbers, and it may be stated that measurements with higher Reynolds numbers are, therefore, not required'.

Prandtl's analysis assumes that the actual form of the velocity profile in the near-wall and core regions is unimportant. In the near-wall region, the mass flux is negligible for Reynolds numbers above $\sim 100\times10^3$, and consequently, the error introduced by neglecting the true form is probably small. In the core region, the error caused by neglecting the deviation of the velocity profile from the log law (the 'wake') is expected

to be significant. However, if the wake is independent of Reynolds number, then the difference between the velocity given by (6) and (5) is independent of Reynolds number, and when integrated across the core of the pipe, the result is a constant. The additive constant in (12), therefore, also accounts for the mass flux in the core region of the pipe. Consequently, Prandtl's relation assumes complete similarity of the mean velocity profile and moderately high Reynolds numbers. The scaling of the friction factor will be further investigated in §6.

Despite the conventional wisdom embodied in the log law, there is still considerable debate over the existence of a log law, the value of the log law constants and their Reynolds number dependence, if any. Barenblatt (1993), for example, proposed a power law with empirical constants that depend on Reynolds number for the velocity profile in the overlap region. A comparison between Barenblatt's theory and the experimental data presented here is given in Zagarola, Perry & Smits (1997). Other workers have attempted to explain an apparent Reynolds number dependence of the constants using higher-order corrections to the classical log law. The work of Tennekes (1968), Afzal & Yajnik (1973), Long (1979), and George, Castillo & Wosnik (1997) fall into this category.

The lack of a consensus on the scaling in the overlap region, or even the existence of an overlap region, can be partly attributed to the lack of adequate experimental data. Although pipe flow has been one of the most extensively studied flows, it is difficult to find data across a wide enough range of Reynolds numbers so that subtle Reynolds number effects can become apparent and basic scaling dependencies can be unambiguously established. Among the most commonly cited experiments in smooth pipes are those by Stanton (1911), Nikuradse (1932), Deissler (1950), Laufer (1954), Townes *et al.* (1972), Perry & Abell (1975), Dickinson (1975), and Toonder & Nieuwstadt (1997). Of these experiments, the only one that covers a significant range of Reynolds numbers is the one performed by Nikuradse which covers three orders of magnitude in Reynolds number. Consequently, Nikuradse's data have become the metric by which theories have been established and judged.

Nikuradse's data have also been the subject of intense scrutiny, and this scrutiny has revealed inconsistencies and uncertainties in his data. The inconsistencies have been well documented (Hinze 1964; Zagarola 1996), and will not be reviewed here. Instead, we will attempt to quantify the uncertainties in his data by examining the random errors in his measurements.

In his 1932 paper, Nikuradse reported 141 friction factor measurements and only 16 velocity profile surveys. The large number of friction factor measurements lends itself to statistical analysis. The standard deviation between Prandtl's friction factor formula (equation (12)), which is based on a least-squares approximation of Nikuradse's data, and the data is approximately $\pm 4\%$ (95% confidence interval), and the largest discrepancy exceeds $\pm 6\%$. If we assume that the uncertainty in the average velocity is negligible, then the uncertainty in u_τ is no less than $\pm 2\%$, half the uncertainty in the friction factor data, since $u_\tau/\bar{U} \propto \lambda^{1/2}$. These uncertainties are quite large, and it is doubtful that differences in log law constants or the difference between a log law and a power law can be discerned without more accurate data. For example, (6) can be used to show that the additive constant in the log law, B, varies by an amount ± 0.4 ($\pm 8\%$) at $y^+ = 100$ for a $\pm 2\%$ variation in u_τ.

The inconsistencies and uncertainties in Nikuradse's data underscore the importance of a new experiment that permits accurate measurements over a large range of Reynolds numbers. The results presented in this paper include measurements of the mean velocity profile and pressure drop for 26 different Reynolds numbers between

31×10^3 and 35×10^6. The strength of the conclusions formed from these results rests on the uncertainties in the measurements, and therefore these considerations occupy a significant fraction of this paper. The experimental facility is described in §2, the measurements are described in §3, and the corrections to the measurements and the uncertainty of the measurements are described in §4. For additional details on each, see Zagarola (1996).

2. Experimental facility

A pipe flow apparatus was constructed to enable very accurate measurements across a wide range of Reynolds numbers, up to very large values. High Reynolds numbers were achieved at a moderate cost by using compressed air at ambient temperatures as the working fluid, thereby decreasing the kinematic viscosity by over two orders of magnitude as compared to air at STP. The maximum static pressure for these measurements was 187 atm. The facility was closed loop and the test pipe was contained inside high-pressure piping. The test pipe had a nominal diameter of 129 mm, a length of $202D$ and included two test sections for measurements of the velocity profiles.

A diagram of the facility is shown in figure 1. The facility was filled with high-pressure air supplied from an external reservoir (not shown). After filling, recirculating flow was produced by an impeller located in the pumping section. The flow rate was varied by changing the rotational speed of the impeller between 500 and 3700 r.p.m. The rotational speed was controlled to better than $\pm 0.25\,\%$. At the exit of the pump, a water-cooled, shell-and-tube heat exchanger controlled the temperature of the flow. By varying the coolant temperature, all measurements were performed at temperatures between 295 K and 300 K. The temperature during a single survey varied by less than ± 0.5 K. From the heat exchanger, the flow continued along the back leg of the circuit, and after two 90° bends the flow entered a flow conditioning section.

The flow conditioning section consisted of two aluminium honeycombs and a contraction with a 4:1 area ratio. The length-to-diameter ratio of the honeycomb was eight which has been shown to virtually eliminate swirl and other lateral velocities (Mehta & Bradshaw 1979). The overall reduction in the variation of the mean velocity through the flow conditioning section and the contraction was estimated to be 94 %. At the exit of the contraction, the flow entered the test pipe (described in §§2.2 and 2.3). At the end of the test pipe, a diffuser increased the flow area to that of the second 180° bend leading to the air pump inlet. The area ratio of the diffuser was 4:1 and the half-angle was 2.4°. The pressure recovery of the diffuser was estimated to be 0.81 (McDonald & Fox 1966).

2.1. *Flow development length*

A flow is fully developed when all mean flow quantities (i.e. velocity field and pressure gradient) and all turbulence quantities (i.e. $\overline{u^2}$, spectra, skewness, flatness, etc.) are independent of streamwise location. For our purposes, we need only the mean flow to be fully developed, which is a much less stringent criterion, but the pipe was designed to attain fully developed flow in the strictest sense. Previous experiments in pipes and channels have shown that for lower Reynolds numbers (of order 10^5) an entrance length of approximately $70D$ to $100D$ is necessary to satisfy this criterion. For example, Abell (1974) verified the fully developed condition at a Reynolds number of 300×10^3 by comparing streamwise turbulence intensity profiles and mean velocity profiles at $71.9D$ and $86.2D$ downstream of the tripping device. To establish the development

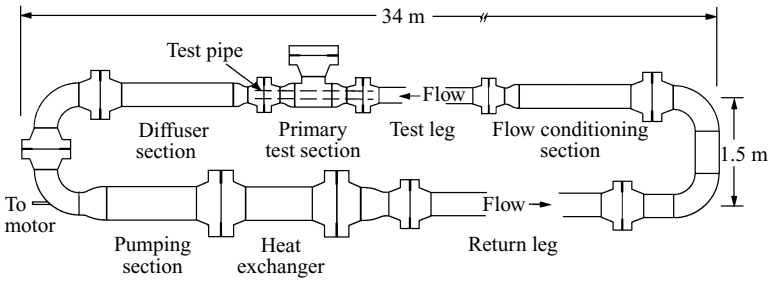

FIGURE 1. A diagram of the experimental facility. The flow is counter clockwise.

length at higher Reynolds numbers, we can divide the development length into three parts: a laminar-to-turbulent transition length (L_0), a turbulent boundary layer development length (L_1) and a large-eddy development length (L_2), and we can investigate the Reynolds number dependence of each part.

The transition length L_0 will depend on the length Reynolds number Re_L since no tripping device was used at the inlet of the test pipe. A reasonable value for Re_L with low levels of free-stream turbulence is 2×10^5. Hence $L_0/D \approx 2\times10^5/Re$. The maximum value of L_0 therefore occurs at the lowest Reynolds number investigated, 31×10^3, where $L_0/D < 7$. At high Reynolds numbers the transition length is considerably smaller.

The turbulent boundary layer development length (L_1) is the length required for the boundary layers to meet at the centre of the pipe. If we neglect the mild favourable pressure gradient and the transverse curvature of the pipe wall, a zero-pressure-gradient estimate indicates that the development length is inversely proportional to the skin-friction coefficient. Hence

$$L_1/D \approx C_1/\lambda, \tag{13}$$

where C_1 is an empirical constant.

After the boundary layers meet, an additional length is required for the turbulence to become fully developed (L_2). The scale that will take the longest length to develop is the large-scale streamwise structure with a characteristic time of D/u_τ. If we assume that the structure is convected with the average velocity of the flow, then L_2 should follow the relationship $L_2/D \sim \bar{U}/u_\tau$ or

$$L_2/D \approx C_2/\lambda^{1/2} \tag{14}$$

where C_2 is another empirical constant.

The upper value of the development length occurs if the three parts are taken to be independent. If we neglect the transition length, the overall development length is a weak increasing function of Reynolds number, given by

$$L/D \approx C_1/\lambda + C_2/\lambda^{1/2}. \tag{15}$$

An estimate for C_1 and C_2 can be made from the channel flow results of Dean & Bradshaw (1976). At a Reynolds number of 10^5, the shear layers met at approximately 30 channel heights downstream of the tripping device and the flatness profiles were independent of streamwise position at approximately 67 channel heights.† Therefore,

$$L/D \approx 0.5/\lambda + 5/\lambda^{1/2}. \tag{16}$$

† The estimates of L_1 and L_2 represent an average of the last measurement location where the flow did not satisfy a development criterion and the first measurement location where the flow satisfied a development criterion.

The development length predicted from (16) is consistent with the pipe flow measurements by Abell (1974), who found that at a Reynolds number of 300×10^3, the overall development length (L) was $72D$ compared to $78D$ as predicted by (16).

Equation (16) predicts an increase in development length from $78D$ to $131D$ when the Reynolds number increases from 300×10^3 to 40×10^6. The measurements presented here were all taken at least $164D$ downstream of the contraction exit, and therefore the flow was believed to be fully developed for all Reynolds numbers.

2.2. *Surface finish*

A surface is usually considered smooth if the equivalent sand-grain roughness height (k_s) is less than five viscous lengths (ν/u_τ), which is approximately the size of the viscous sublayer (Schlichting 1987). That is,

$$k_s/R \leqslant 5/R^+ \tag{17}$$

or equivalently,

$$k_s/D \leqslant 5/Re\,(\lambda/8)^{1/2} \tag{18}$$

for a pipe to be considered smooth. The most severe roughness requirement is at the maximum Reynolds number of 35×10^6. Most machined surfaces are specified with a root-mean-squared roughness, and, as we will show later, for the particular machined and polished surface of our pipe, $k_s \approx 3k_{rms}$. Therefore, for a 129 mm diameter pipe, k_{rms} must be less than 0.21 μm (8.3 μin.) for the surface to be considered smooth at all Reynolds numbers up to 35×10^6.

The surface of the test pipe was carefully prepared to ensure that it was smooth. Consecutive sections of the test pipe were joined together and then honed and polished by a vendor that specializes in these processes. The pipe was then hand polished and inspected. Prior to performing the measurements presented in this paper, a preliminary set of measurements were made to determine the quality of the surface finish. For the preliminary measurements, the section of pipe $54D$ upstream of the primary measurement point was polished to a surface finish of 0.15 ± 0.03 μm r.m.s. The section upstream of that location was polished to a lesser finish somewhere between 0.30 and 0.40 μm. The effect of this discontinuity in roughness was initially considered unimportant, but the preliminary measurements indicated that it could not be ignored for Reynolds numbers greater than 20×10^6. Subsequently, the entire test pipe was re-polished and the surface finish at different points along the pipe was measured independently by three different people using a comparator plate. At each point, the estimate from each person was within ± 0.03 μm of the average value for that point. According to these measurements, the surface finish of the entire test pipe can be conservatively characterized as a 0.15 ± 0.03 μm r.m.s. which corresponds to $k_s^+ = 3.5 \pm 0.7$ at $Re = 35 \times 10^6$. The pipe is therefore hydrodynamically smooth at all Reynolds numbers reported here. The issue of surface roughness will be considered further in §5.

2.3. *Test pipe specifications*

The test pipe was an extruded tube manufactured from 6061-T6 aluminium. It had an outer diameter of 152 mm and a wall thickness of 13 mm (as purchased). The overall length of the test pipe ($202D$) was divided into eight segments to facilitate assembly. Consecutive segments were assembled, aligned, honed and polished to ensure a straight pipe, a precise diameter, a smooth surface and uniform connections. The test pipe had two access ports for measurements of the velocity profiles. The secondary test section was located $160D$ downstream of the contraction exit, and the primary test section was located $196D$ downstream of the contraction exit and $6D$ upstream of the end diffuser.

The pressure gradient was measured between the secondary and primary test section ($164D$ to $189D$).

The diameter of the test pipe was measured at 17 locations along its length. The inner diameter at each location was within ± 0.08 mm of the average diameter at a given location and most were within ± 0.03 mm. This tolerance was independent of angular and longitudinal position, but these measurements were confined to regions within $1D$ of the connections. The pressure gradient and velocity profiles were measured at locations where the diameter of the test pipe was 129.36 ± 0.08 mm.

The test pipe was round along the entire length, but the average diameter varied slightly (0.8 mm or 0.6% maximum variation). The variation of the inner diameter needed to be small to prevent changes in the flow due to acceleration or deceleration. Two types of variation of the diameter could have affected the measurements in the test pipe. The first type is called waviness, which had a typical wavelength of 2–3 diameters (estimated by examining the variation of the surface reflection of the pre-honed test pipe) and is caused by the fabrication process. The waviness was removed by the honing process. The second type of variation of diameter was caused by re-honing parts of the test pipe to improve connections or remove scratches in the original honed pipe. The re-honing involved a blending process to match slightly different diameters. The transitions in diameter were gradual and were believed to have a negligible affect on the measurements (see Zagarola 1996).

Another consideration was the straightness of the pipe. Variations in straightness will distort the velocity field in a manner similar to the curvature effects encountered in flow around a bend. This analogy suggests finding a radius of curvature (R_0) for the test pipe and applying scaling laws developed for curved pipe flows. For a curved pipe, we can define the parameter

$$\Omega = Re\,(R/R_0)^2, \tag{19}$$

where Re is the conventional Reynolds number for the pipe. Experiments show that when $\Omega \quad 1$, the friction factor in curved pipes is equivalent to the value in straight pipes. After analysing a considerable amount of data from various authors, Ito (1959) concluded that if $\Omega < 0.034$, the curved pipe friction factor relationship coincided with the straight pipe relationship.

The test pipe was aligned with a $32\times$ optical builders level and an alignment target. The straightness of the entire test pipe was determined to be ± 1.9 mm. From this uncertainty, an estimate for the minimum radius curvature is 3000 m, which gives $\Omega \leqslant 0.018$. The pipe was therefore considered sufficiently straight.

The test pipe consisted of eight sections connected by custom-designed couplings that ensured repeatability of the connections. An estimate for the largest mismatch or step at a connection was 0.08 mm. The velocity profiles were measured at a location approximately 8300 step heights behind a connection. To show that the step had a negligible affect on the measurements, an experiment was performed with an artificial step placed in the flow. The artificial step was created using a $\frac{3}{4}$ in. diameter cylinder placed through the wall of the test pipe. The artificial step was 1.7 mm high at the centre and 1.0 mm high at the sides. Velocity profiles were measured at 3400 step heights downstream (4.8 m) of the artificial step at four different Reynolds numbers between 2.7×10^6 and 19×10^6. The differences between the velocity profiles measured with and without the artificial step in the flow were less than the uncertainty in the velocity measurement, and we concluded that the velocity profiles were not affected by the actual steps in the flow.

3. Measurement techniques

The mean-flow measurements consisted of streamwise static pressures and velocity profiles at Reynolds numbers between 31×10^3 to 35×10^6. Each Reynolds number was obtained by varying either the density or the flow rate. The density was approximately proportional to the absolute pressure since the temperature was always near ambient (295 K to 300 K). The absolute pressure inside the pipe was varied between 1 atm and 186 atm and was measured by three calibrated pressure gauges each with a different full-scale range. The absolute pressure measurements had an uncertainty of $\pm 0.3\%$ of the reading. The temperature was measured with a calibrated chromel–alumel thermocouple with an uncertainty of $\pm 0.05\%$ for temperatures near ambient. The density and viscosity were calculated from the absolute pressure and temperature using real-gas relationships (see Zagarola 1996). The uncertainty in the calculated density and dynamic viscosity were $\pm 0.36\%$ and $\pm 0.80\%$, respectively.

The velocity profiles were measured at the primary test section by traversing a 0.90 mm round Pitot probe. For each profile, the velocity was measured at 52 locations between $0.007R$ and $1.5R$. The Pitot probe was aligned with the flow direction to better than $\pm 1°$ which caused an insignificant error due to yaw (see Chue 1975). The Pitot probe measurements were reduced to velocity measurements using the incompressible Bernoulli equation. These measurements were corrected for the velocity gradient effect, finite-size static pressure taps, viscous effects, radial pressure gradient and turbulence according to the methods outlined by Chue (1975). These corrections were small and tended to cancel. In §4, the corrections will be reviewed in more detail and the impact on the measured velocity will be quantified.

The Pitot probe was traversed by a model LM-F5A-P13A positioner manufactured by Compumotor which had a resolution of 0.002 mm and an accuracy of ± 0.013 mm. The position was also measured using a linear potentiometer. The potentiometer measurement had an uncertainty of ± 0.076 mm and was used only as a check on the positioner. The starting position for the probe was found by a capacitance method developed by Muzas (1995), where the Pitot probe tip and test pipe wall served as the two 'plates' of the capacitor. With this method, the outer surface of the Pitot probe could be placed within 0.04 mm of the wall at the start of a survey. The overall uncertainty in the distance from the wall to the centre of the Pitot probe was ± 0.05 mm.

Sixty-two static pressure taps were placed at various locations along the length and circumference of the test pipe. The taps were formed by boring a 0.79 mm diameter hole from the outside of the test pipe radially inwards towards the centre. The pressure gradient was determined from 20 static pressure taps equally spaced over $25D$, in the region between the secondary and primary test section. The uncertainty in the streamwise position for the 20 taps relative to each other was ± 0.1 mm or $\pm 0.001D$.

In figure 2, the static pressure errors for the 20 taps used to measure the pressure gradient are shown for five different Reynolds numbers. The pressure error shown (ΔP_c) is the difference between the pressure measured at a tap and the pressure calculated at that tap by a least-squares approximation of all 20 taps. The pressure errors appear to be randomly distributed and the maximum error occurs at the maximum Reynolds number. The maximum error was approximately equal to τ_w. None of the taps showed the large pressure deviations associated with burrs, and therefore, we believe the holes were approximately uniform. Table 1 lists the static pressure errors (2σ of $\Delta P_e/\tau_w$), the pressure gradient, the correlation coefficient (R_c) and the uncertainty in the pressure gradient estimation (95% confidence interval) for

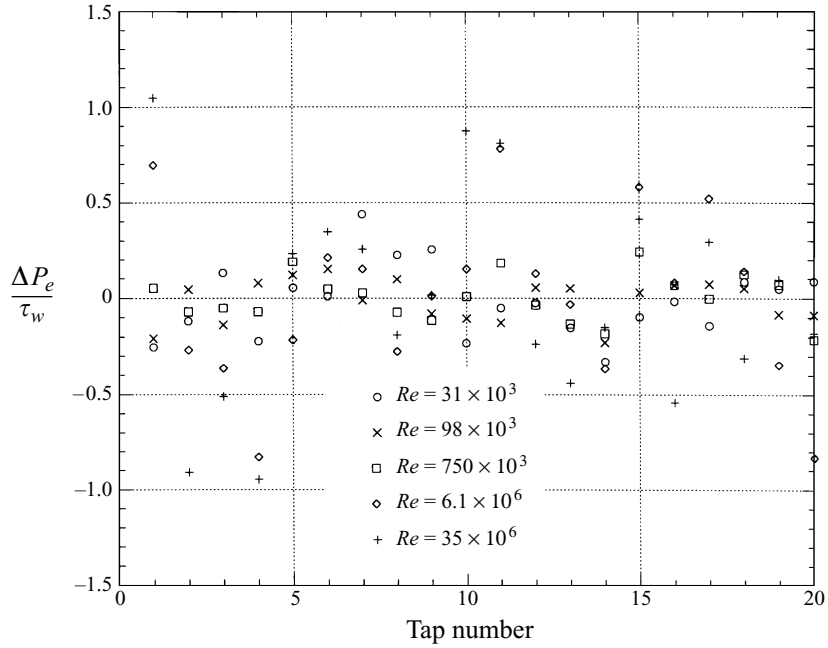

FIGURE 2. A comparison between the static pressure errors for the 20 taps used to measure the pressure gradient. The pressure error is the difference between the pressure measured at a tap and the pressure calculated at that tap by a least-squares approximation using all 20 taps.

Re	2σ for $\Delta P_e/\tau_w$	dP/dx (Pa m^{-1})	R_e	Error (%) dP/dx
32×10^3	0.19	−1.571	0.99998	±0.29
99×10^3	0.11	−11.64	0.99999	±0.17
750×10^3	0.12	−32.67	0.99999	±0.18
6.1×10^6	0.89	−238.2	0.99989	±0.68
35×10^6	1.10	−5176	0.99984	±0.83

TABLE 1. Uncertainty of the static pressure measurements

the Reynolds numbers shown in figure 2. The maximum uncertainty in the estimation of the pressure gradient occurred at the maximum Reynolds number and was ±0.83%.

The Pitot probe and static pressures were both measured as differential pressures. The range of differential pressures encountered in this experiment was approximately five decades, from 1 Pa to 100×10^3 Pa (1.5×10^{-4} p.s.i.d. to 15 p.s.i.d.). Six differential pressure transducers were used to accurately determine the pressure gradient and velocity profiles across the entire range of Reynolds numbers. Four transducers were located inside the pressure vessel to minimize the stresses acting on the instruments and were used for surveys at static pressures above atmospheric. The other two transducers were located outside the pressure vessel and were used for tests at atmospheric pressure. The differential pressure transducers were calibrated by comparison with a manometer standard or a dead-weight tester, depending on its range, and have an uncertainty of less than ±0.40% of the reading.

The data were acquired through use of a data acquisition system conforming to the CAMAC standard and a laboratory computer. The measurement devices output

analog voltages which were offset and amplified as required by a calibrated differential amplifier. The A/D converter had 12-bit resolution and a voltage window of ± 5 V (2.4 mV/count). The resolution of the conversion had no effect on the accuracy of the measurements. For each data point, four channels – the differential pressure, the position, the absolute pressure and the temperature – were sampled for nominally 30 s.

The average velocity was calculated by numerically integrating the velocity profile. The integration limits were the data point closest to the wall and the centreline. The average velocity was corrected for the unresolved region near the wall. Here the velocity profile was represented using the relation proposed by Spalding (1961). To find the average velocity, Spalding's relation was integrated from the wall to the first data point, and this value was added to the value attained from integrating the remaining profile to the centreline. The values of κ and B used in this correction were 0.44 and 6.3 which were found to adequately represent the velocity profile in the overlap region (see Zagarola *et al.* 1996). Note that the difference in the average velocity when using other values for κ and B was small (e.g. for $\kappa = 0.41$ and $B = 5.2$, the average velocity changed by less than 0.09 % for $Re = 35 \times 10^6$). The difference between the average velocity calculated using Spalding's relation and a linear relation for the correction had a maximum value of 0.4 % which occurred at the maximum Reynolds number.

The centreline velocity was found by a least-squares approximation of the velocity profile near the centreline. This method was preferred over using the maximum velocity as the centreline velocity because this method reduced the random error associated with an individual velocity measurement. In practice, the difference between the maximum velocity and the centreline velocity found by this method was less than 0.2 % of the centreline velocity.

To investigate the symmetry of the flow, the static pressure was measured at eight positions, uniformly spaced around the circumference of the pipe and located approximately $6D$ upstream of the primary test section. We investigated two different Reynolds numbers, 190×10^3 and 12×10^6. For each Reynolds number, the variation in the circumferential static pressure was comparable to the uncertainty in the streamwise static pressure (see table 1).

In addition, the azimuthal variation in the wall shear stress was investigated using eight Preston probes, equally spaced around the circumference of the pipe, at a location approximately $2D$ downstream of the primary test section. Two different Reynolds numbers were investigated, 190×10^3 and 12×10^6. For both Reynolds numbers, the variation in the Preston probe pressure was less than 1.7 %, randomly distributed around the circumference. This variation can be attributed to differences in Preston probe geometry. The maximum variation can be compared to similar experiments such as the one performed by Dickinson (1975) in which the variation was as great as ± 4 %.

The velocity measurements at positions between $-0.25 < r/R < 0.25$ were also used to investigate the symmetry of the flow at all Reynolds numbers. For most Reynolds numbers, there appeared to be a slight asymmetry in the profile since the peak velocity occurred at a position approximately 0.5 % of the radius past the centreline. The asymmetry can be interpreted as an error in either position or velocity. If our estimate for the uncertainty in the position is correct (± 0.07 % of R for positions near the centreline), then this asymmetry is most likely caused by small systematic errors in the velocity. Even so, this asymmetry is within the uncertainty bounds for the velocity measurements and will not change the conclusions drawn from these measurements.

In summary, the flow was found to be azimuthally symmetric within the uncertainty of the measurements.

4. Corrections to the measurements

Corrections to the velocity measurements that were considered are due to the velocity gradient, viscosity, turbulence, radial static pressure gradient, compressibility and probe tip/strut interference. It will be shown that all corrections are small and tend to cancel. A comprehensive review of these effects and corrections is given in Chue (1975).

4.1. *Velocity gradient*

When measuring velocities with a Pitot probe in a uniform stream, the velocity measured is that at the geometric centre of the probe. When the probe is used to measure the velocity in a shear layer, the velocity measured is not that at the centre of the probe, but is different due to two effects. First, the velocity is proportional to the square-root of the dynamic pressure, so when the dynamic pressure is averaged over the cross-sectional area of the probe, the calculated velocity is different from that at the centre. Secondly, the presence of the Pitot probe deflects the streamlines in a manner which causes the Pitot probe to measure a velocity different from that at the centre. Chue (1975) shows that the first correction is small compared to the second. A correction for the second effect (generally called the velocity gradient effect) can be made by either reducing the velocity at a given point or displacing the point towards the region of higher velocity (i.e. shift the point further from the wall). Most investigators have chosen to displace (shift) the position.

The experiments by MacMillan (1956), Livesey (1956), Davies (1958), Patel (1965) and Ozarapoglu (1972) showed displacements (Δy) of 8% to 16% of the outer diameter (D_{probe}) of the Pitot probe, and that this correction was independent of the inner diameter of the probe, velocity gradient and probe Reynolds number. This correction is usually written as

$$\Delta y/D_{probe} = \epsilon, \tag{20}$$

where ϵ is taken to be between 0.08 and 0.16.

The correction given by (20) cannot continue in regions where the velocity gradient is small (e.g. the core region of a pipe). Clearly, as the velocity gradient becomes small the displacement should tend towards zero. Chue (1975) analysed an extensive set of experimental and theoretical investigations on free shear flows and concluded that the correction for both free and wall-bounded shear flows should depend on the velocity gradient. He attributed the constant displacement that some investigators found to the limited range of velocity gradients encountered in their experiments (i.e. limited range of Reynolds numbers and limited range of wall-normal positions). Chue suggested a correction method for wall-bounded shear flows which can be represented by

$$\Delta y/D_{probe} = \epsilon(\alpha) \approx 0.18(\alpha - 0.17\alpha^3), \tag{21}$$

where α is the shear parameter.

If the mean velocity gradient is known, the shear parameter can be calculated according to

$$\alpha = \frac{1}{U_c}\frac{\mathrm{d}U}{\mathrm{d}y}\bigg|_c \frac{D_{probe}}{2}, \tag{22}$$

where the subscript c denotes the quantity evaluated at the centre of the Pitot probe. The shear parameter has a maximum value near the wall and decreases to zero at the centreline. For positions within the viscous sub-layer, the shear parameter is unity and the shift in the position given by (21) is $0.15 \times D_{probe}$. This is the same value as the one

obtained by MacMillan and verified by Patel. Equation (21) was used to correct the measured positions.

The displacement correction affects the estimate of the average velocity and log-law constants. The correction given by (21) changed the average velocity by a maximum of 0.15% which occurred at low Reynolds numbers. The effect of the displacement correction on κ was estimated to be less than 0.6% for all Reynolds numbers above 300×10^3. The impact on κ at lower Reynolds numbers was not determined because it is doubtful that a log law exists over a large enough range of y^+ to make an accurate estimate. The maximum change of the additive constants, B and B^*, was 2% and 3%, respectively, which occurred at the maximum Reynolds number. In contrast, it was found that the commonly used MacMillan correction had a much larger and we believe spurious effect on the constants (on the order of 5% for κ and 20% for B and B^*).

4.2. *Other corrections*

In our experiment, the minimum probe Reynolds number occurred at the minimum pipe Reynolds number when the probe was near the wall. Here the probe Reynolds number was approximately 40. For a probe Reynolds number of 100, the data examined by Chue (1975) indicate that viscous effects will increase the measured velocity by 0.5% over the true value. In our experiment, most measurements were at significantly higher probe Reynolds numbers than 100 so the correction for viscous effects was typically negligible.

Turbulence affects the readings of a Pitot probe by increasing the total pressure sensed at the tip and varying the static pressure across the radius of the pipe. For y^+ greater than approximately 50, Dickinson (1975) showed that the combined effect due to turbulence can be approximated by

$$\frac{U - U_m}{U_m} = -\frac{\overline{u^2}}{2U_m^2}, \tag{23}$$

where U_m is the measured velocity and $\overline{u^2}$ is the mean-squared velocity fluctuation. Equation (23) shows that the effect of turbulence is to increase the measured velocity above the true velocity. The error in the measured velocity is largest in the region near the wall, since the fluctuating velocity is the largest percentage of the mean velocity. It can be shown that the velocity correction for turbulence was typically less than 0.5% of the local velocity. The impact of this correction on the average velocity was largest at low Reynolds number and was less than 0.6%. For higher Reynolds numbers, the impact was typically less than 0.3%.

The velocity measurements were corrected for errors in the static pressure measurements caused by finite-size static pressure taps in accordance with the results obtained by Shaw (1959). Errors due to finite-size static pressure taps cause the measured velocity to be smaller than the true velocity. The maximum correction was less than 0.5% of the uncorrected average velocity. Note that this correction does not affect the measured static pressure gradient since all static taps had a similar geometry.

The interference caused by the strut and probe tip can affect the static pressure measured at the wall and the total pressure measured at the Pitot probe tip. The experimental data given in Chue (1975) can be used to show that the error in the measured velocity was less than 0.03% for the Pitot probe geometry used in this experiment. Consequently, no corrections for strut or probe tip interference were applied to the measurements.

Compressibility can affect the velocity measurements in several ways. All the corrections were small since the maximum Mach number encountered in this

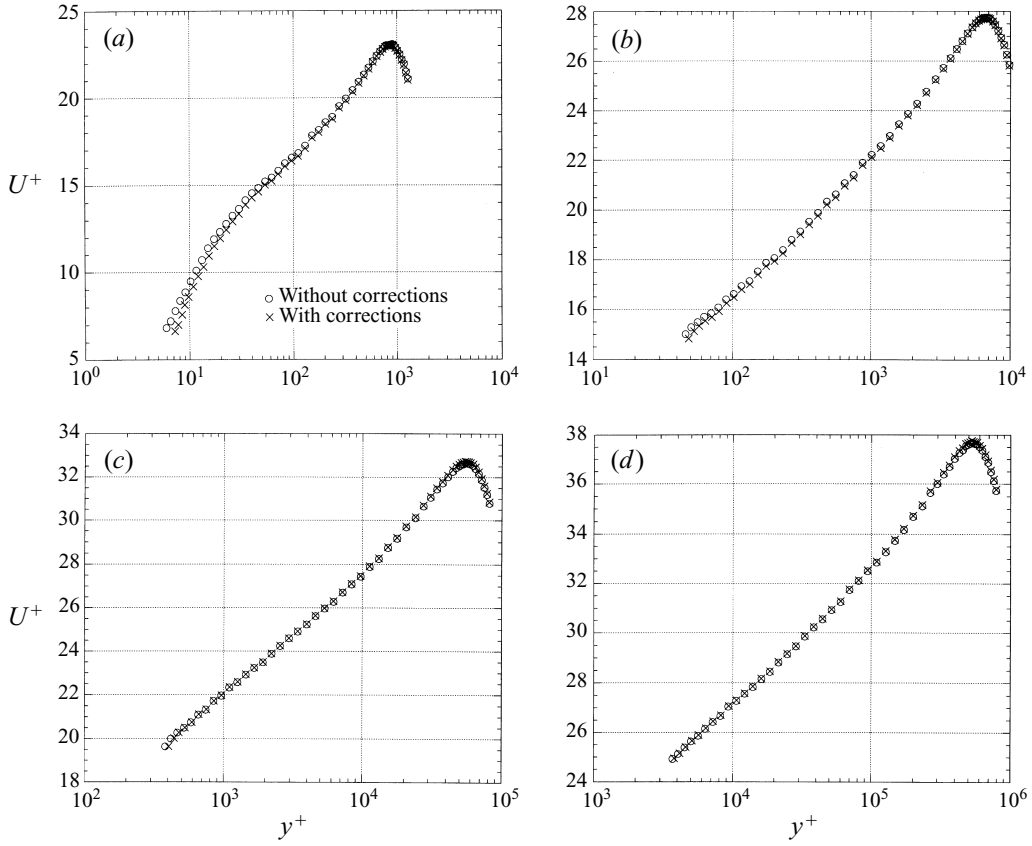

FIGURE 3. Plots showing the effect of all corrections on the velocity profiles for Reynolds numbers of (*a*) 31×10^3, (*b*) 310×10^3, (*c*) 3.1×10^6 and (*d*) 35×10^6.

experiment was approximately 0.07. The maximum difference between the measured and true velocity due to compressibility was less than 0.02%, and therefore no corrections for compressibility were made.

4.3 *Effect of all corrections*

In summary, the velocity profiles were corrected for the errors caused by the velocity gradient, viscosity, radial static pressure gradient, turbulence and finite-size static pressure taps. The position values were corrected using the formula derived from Chue (1975) before applying the other corrections. Figure 3(*a–d*) shows comparisons between the uncorrected velocity profiles and the corrected velocity profiles for four different Reynolds numbers. The effect of these corrections was negligible for the velocity profiles at Reynolds numbers of 3.1×10^6 and 35×10^6. At $Re = 310 \times 10^3$, the corrections were only important near the wall, and at $Re = 31 \times 10^3$, the corrections were important for most of the velocity profile. The effect of these corrections on the average velocity is shown in figure 4. The maximum correction occurred at the lowest Reynolds number investigated and was less than 1%. At high Reynolds numbers ($Re > 2 \times 10^6$), the correction was negligible (less than 0.1%).

The largest difference between the form of the corrected and uncorrected velocity profiles occurs at the lowest Reynolds number. To examine the accuracy of our correction method, the velocity profiles were compared with other experimental velocity profiles which did not require these corrections. The laser Doppler anemometry

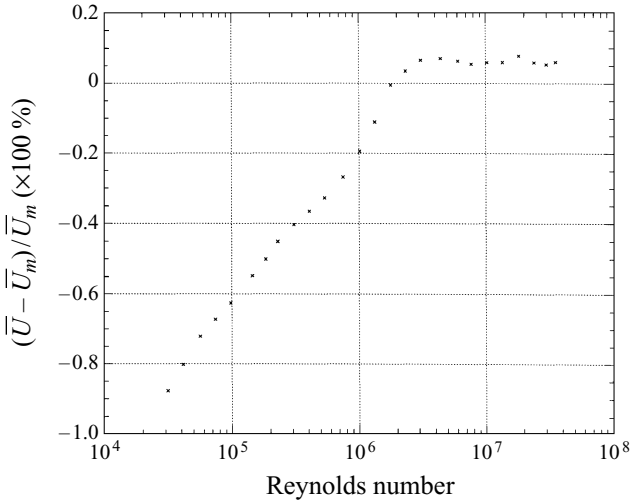

FIGURE 4. A comparison between the measured and corrected average velocity as a function of Reynolds numbers.

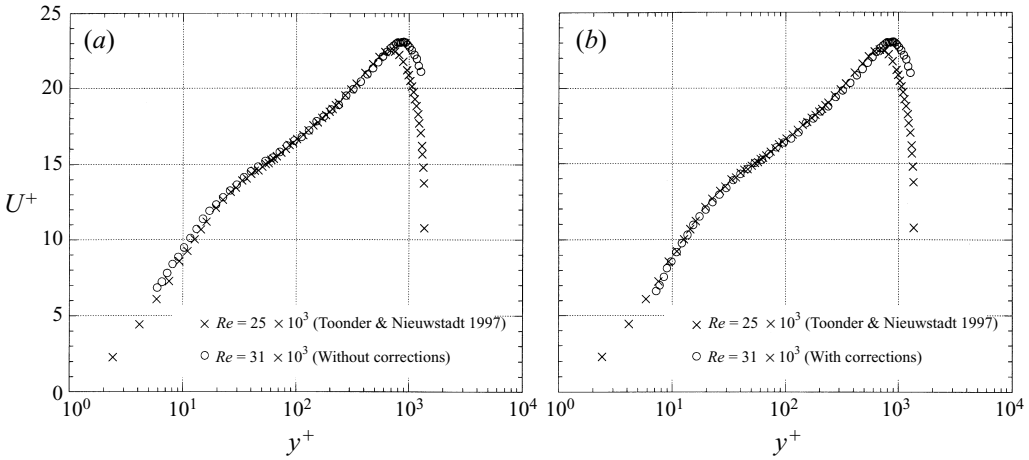

FIGURE 5. Comparisons between the velocity profile measured here with a Pitot probe and the velocity profile measured by Toonder & Nieuwstadt (1997) with an LDA system. In (*a*) the Pitot probe measurements were not corrected, while in (*b*) the Pitot probe measurements were corrected for the errors discussed in §4. The size of the symbols is representative of the uncertainty in our measurement of U^+.

(LDA) measurements by Toonder & Nieuwstadt (1997) were used for this comparison. The pipe used in their experiment had a diameter of 40 mm and a length of 34 m. The velocity profiles were measured at a streamwise location $850D$ downstream of the tripping device, so that there is no question that the flow was fully developed. The friction velocity was determined from the static pressure measured at two points which were separated by at least $250D$. Toonder & Nieuwstadt corrected their measurements for a finite-size measuring volume, but this correction was presumably small since the size of the measuring volume was only 20 μm (0.1 % of the radius) in the wall-normal direction.

Figures 5(*a*, *b*) and 6 show the mean velocity profile that Toonder & Nieuwstadt measured at their highest Reynolds number of 25×10^3 compared to the mean velocity

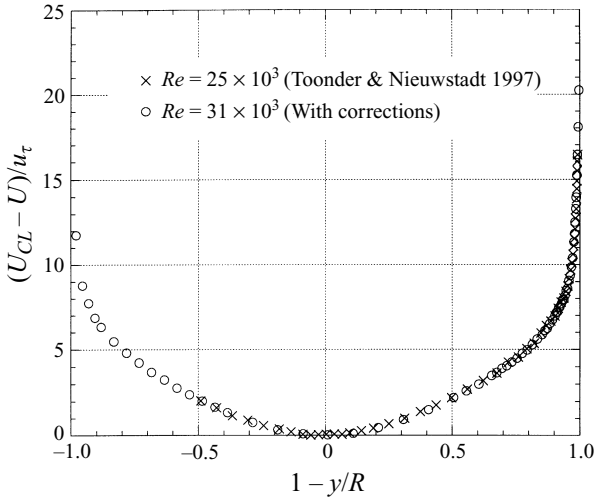

FIGURE 6. A comparison between the velocity profile measured here with a Pitot probe and the velocity profile measured by Toonder & Nieuwstadt (1997) with an LDA system. The Pitot probe measurements were corrected for the errors discussed in §4.

Quantity	Variable	Uncertainty (% unless noted)
Differential pressure	$P_2 - P_1$	± 0.40
Absolute pressure	P_a	± 0.30
Absolute temperature	T_a	± 0.05
Wall-normal position	y	± 0.05 mm
Density	ρ	± 0.36
Dynamic viscosity	μ	± 0.80
Kinematic viscosity	ν	± 0.88
Velocity	U	± 0.35
Average velocity	$\bar{U}$	± 0.30
Friction velocity	u_τ	± 0.45
Centreline velocity	U_{CL}	± 0.30
Pressure gradient	$\mathrm{d}P/\mathrm{d}x$	± 0.83
Radius or diameter	R or D	± 0.06
Normalized wall-normal position @ centreline (outer scaling)	η	± 0.07
Normalized wall-normal position @ 1st point (outer scaling)	η	± 11
Normalized wall-normal position @ centreline (inner scaling)	y^+	± 0.99
Normalized wall-normal position @ 1st point (inner scaling)	y^+	± 11
Normalized velocity (inner scaling)	U^+	± 0.57
Friction factor	λ	± 1.1
Reynolds number	Re	± 0.93
Kármán number	R^+	± 0.99

TABLE 2. Uncertainty estimates of key quantities

profile that we measured at our lowest Reynolds number, 31×10^3. Figure 5(*a*) shows the uncorrected data, and figures 5(*b*) and 6 show the corrected data. In figure 5(*a*, *b*) the velocity profiles are normalized using inner scaling variables. For this scaling, the difference between the velocity profiles near the centreline is due to the difference in Reynolds number. The uncorrected velocity profile is significantly different from the velocity profile measured by Toonder & Nieuwstadt, especially near the wall. Even in

the overlap region, the shapes of the velocity profiles are slightly different. However, the corrected velocity profiles are in excellent agreement. In figure 6, the corrected velocity profile is also plotted using outer layer variables. Again, the corrected velocity profile is in excellent agreement with the data of Toonder & Nieuwstadt, validating our correction procedures at low Reynolds numbers where the errors are the largest.

4.3. *Uncertainty analysis*

Estimates for the uncertainties of the measured and derived quantities are given in table 2. The uncertainties for the derived quantities were calculated using the method outlined by Kline and McClintock (see Holman 1989 for a summary of this method). All values given in table 2 represent a 95% confidence interval, and they were established using the Reynolds number which produced the largest uncertainty. Therefore, for many quantities (e.g. the pressure gradient), the estimated uncertainty was considerably larger than the actual uncertainty at many Reynolds numbers. Also, the uncertainty analysis assumes that the corrections applied to the measurements had an uncertainty of $\pm 25\%$, but it does not account for any systematic errors. When systematic errors were encountered, the sources of these errors were eliminated and the measurements were repeated.

5. Surface roughness

Preliminary measurements of the mean velocity profiles and the friction factor were made at 28 different Reynolds numbers. These surveys were performed before the test pipe was polished to the surface finish used during the final surveys. The preliminary surveys indicated that the surface of the test pipe was not adequately smooth for Reynolds numbered above approximately 20×10^6.

Figure 7 shows a comparison between the friction factor before and after the test pipe was polished a second time. The size of the symbols in figure 7 is representative of the uncertainty in the friction factor. For Reynolds numbers below 24×10^6, the two sets of measurements are in good agreement, but for Reynolds numbers greater than this value, the friction factor was larger before the second polishing. Before the second polishing, the surface of the test pipe had a 0.30 to 0.41 μm r.m.s. finish for the upstream portion of the test pipe (0 to 142D), and a 0.15 μm r.m.s. for the downstream portion (142D to 196D). After the second polishing, the entire surface had a 0.15 ± 0.03 μm r.m.s. finish. From the data presented in figure 7, it can be concluded that the reduction in the roughness height (i.e. improved surface finish) decreased the friction factor for Reynolds numbers greater than 24×10^6. Although these results are encouraging, they do not prove that the surface was hydrodynamically smooth at the highest Reynolds numbers after the test pipe was polished a second time.

To establish the smoothness of the pipe, we need to examine the velocity profiles. One consequence of roughness is a decrease in the additive constant B in the log law (see Hama 1954; Clauser 1956; Schlichting 1987). The additive contant was found from the final set of measurements using the following procedure. First, the value of von Kármán's constant (κ) was found from a curve fit of the friction factor data (the procedure is described in §6). The value of von Kármán's constant was found to be 0.436. Next, for each Reynolds number, B was calculated for each data point in the logarithmic region which was shown to exist for $600 < y^+ < 0.07\,R^+$ (see §7). The data points near the wall ($y/R < 0.01$) were neglected due to the relatively large uncertainty in their positions, and only Reynolds numbers with at least six data points in the assumed logarithmic region were analysed. At the higher Reynolds numbers, 15 data

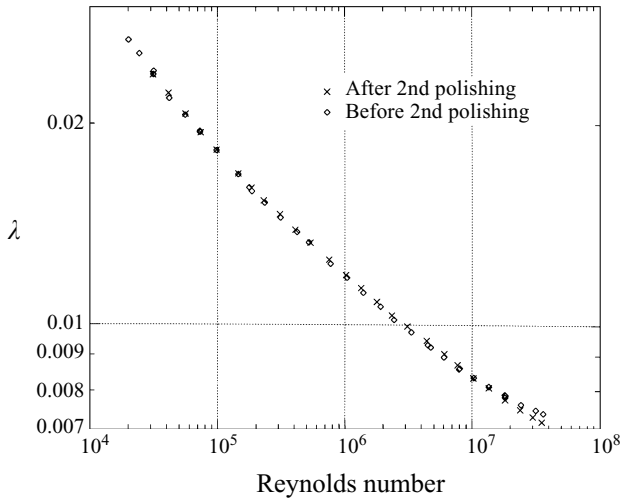

FIGURE 7. A comparison between the friction factor measured before and after the test pipe was polished a second time. The size of the symbols is representative of the error in the friction factor ($\pm 1.1\,\%$).

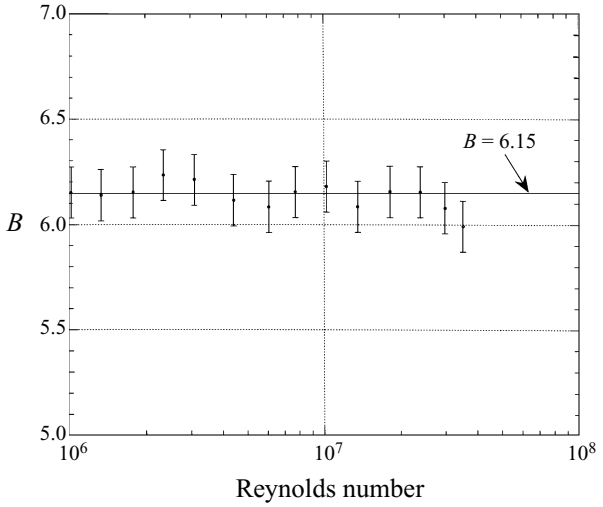

FIGURE 8. The additive constant B in the log law as a function of Reynolds numbers. The calculation of B assumed a fixed value for von Kármán's constant ($\kappa = 0.436$). The data used to calculate B were measured after the test pipe was polished a second time. The uncertainty in B is ± 0.12.

points were in the assumed log region. The values of B at each Reynolds number were averaged (no-weighting) and the results are shown in figure 8. Also shown is an estimate of the uncertainty in B (± 0.12) which is mostly due to the uncertainty in u_τ.

The additive constant has an average value of 6.15 with a standard error of 0.02 when the highest Reynolds number is neglected. Note that in Zagarola & Smits (1997) we gave the value of B as 6.13 with a standard error of 0.04. The new value is based on a refined analysis of the log-law limits which is presented in §7.

At the highest Reynolds number, there is a slight decrease in B. If we accept the trend of B at the highest Reynolds number to perhaps display the weak effects of roughness,

then the change in B from its global average value may be used as a measure of the roughness. For $Re = 35 \times 10^6$, the decrease in B from its global average value is 0.15 ($\approx$ 6.15–6.00). From analysis of his rough pipe data, Nikuradse (1933) developed a correlation for the change in B at the 'inception' of roughness which is

$$\Delta B = 1.1\text{–}2.3 \log k_s^+, \tag{24}$$

where k_s^+ is the non-dimensional equivalent sand-grain roughness. According to Nikuradse, the range of validity of (24) is $3.5 < k_s^+ \leqslant 7.1$, but comparison with his data shows good agreement to $k_s^+ = 3.0$ where $\Delta B = 0$. For $k_s^+ < 3.0$, the roughness height has no impact on B, and presumably no impact on the velocity distribution outside the viscous sublayer.

For a 0.15 change in B, (24) gives $k_s^+ = 3.5$ which is actually in the smooth regime as defined by Schlichting (1987). We can then infer that $k_s \approx 3k_{rms}$ since $k_{rms}^+ = 1.2$. At the next highest Reynolds number, we then have $k_s^+ = 3.0$, and we expect from Nikuradse's rough-pipe data that the effect on the additive constant is negligible, and this conclusion is consistent with the behaviour shown in figure 8. It appears that the effects of roughness on the data are negligible, except for the highest Reynolds number where it is possible that the additive constant has been reduced slightly from 6.15 to about 6.00, although strictly speaking, the change is commensurate with the uncertainty in B (± 0.12).

6. Friction factor results

The friction factor relationship proposed by Prandtl can be derived from the integration of the mean velocity profile (see §1). This relation can be written as

$$1/\lambda^{1/2} = C_1 \log (Re\, \lambda^{1/2}) + C_2, \tag{25}$$

where C_1 and C_2 are coefficients which may or may not depend on Reynolds number. If $C_1 = 2.0$ and $C_2 = -0.8$, then (25) is the same as that derived by Prandtl from the smooth-pipe data of Nikuradse (1932). The argument that the coefficients in (25) are independent of Reynolds number is predicated on two assumptions: (i) a log law exists with coefficients that are independent of Reynolds number, and (ii) the contribution of the near-wall region (say $y^+ < 50$) to the average velocity is negligible. For low Reynolds numbers (say $Re < 100 \times 10^3$), the ratio of scales R^+ is still relatively small, and it is probable that the interaction between the wall and core regions is significant. Here a logarithmic overlap region may not exist. At higher Reynolds numbers, local similarity may exist and the coefficients in the log law may be independent of Reynolds number. Even so, the contribution to the average velocity from the near-wall region may be significant, and C_2 may still depend on Reynolds number.

To identify the relationship between the mean velocity profile and the friction factor, the coefficients in (25) are written in terms of the log-law coefficients (B, B^* and κ). That is,

$$C_1 = \frac{1}{\kappa 2\sqrt{2} \log (\mathrm{e})}, \tag{26}$$

$$C_2 = \frac{B}{2\sqrt{2}} - \frac{1}{\kappa}\left[\frac{\log (4\sqrt{2})}{2\sqrt{2} \log (\mathrm{e})} + \frac{3}{4\sqrt{2}}\right] + C_3 - C_4, \tag{27}$$

where e is the exponential constant (e $\approx$ 2.718), and C_3 and C_4 are coefficients which account for the difference between the actual velocity and velocity predicted by the log

law when extrapolated into the core and near-wall regions, respectively. Note that C_3 and C_4 are always greater than zero and that the functional dependence of C_4 is approximately $1/R^+$ (this will be quantified later in this section). When R^+ is large, C_4 must go to zero because the size of the near-wall region (say $y^+ < 50$) becomes a negligible fraction of the radius.

Equation (26) can be used to determine κ without evaluating the slope of the velocity profile using discrete data points or without curve fitting each velocity profile over a limited range of y^+. This appears to be the most accurate method to determine κ provided that the Reynolds number dependence of the near-wall region is properly accounted for in C_4. If C_1 is independent of Reynolds number, then κ must also be independent of Reynolds number. There is no equivalent method to determine B since C_3 and C_4 are also unknown, and the velocity profiles must be used to determine B. If C_1 and C_2 are independent of Reynolds number and R^+ is large, then both B and C_3 must be independent of Reynolds number.

Besides using the average velocity, the resistance in a pipe can be represented in terms of the centreline velocity (U_{CL}). If (6) is added to (7), we obtain

$$U_{CL}/u_\tau = \frac{1}{\kappa}\ln R^+ + B + B^*. \tag{28}$$

For comparison with (25), equation (28) can be re-written as

$$U_{CL}/u_\tau = 2\sqrt{2}[D_1 \log(Re\,\lambda^{1/2}) + D_2], \tag{29}$$

where D_1 and D_2 are coefficients. These coefficients can also be written in terms of the log-law coefficients as

$$D_1 = \frac{1}{\kappa 2\sqrt{2}\log(\mathrm{e})}, \tag{30}$$

$$D_2 = \frac{B+B^*}{2\sqrt{2}} - \frac{1}{\kappa}\left[\frac{\log(4\sqrt{2})}{2\sqrt{2}\log(\mathrm{e})}\right]. \tag{31}$$

Consequently, C_1 and D_1 are expected to be equal. Equation (30) provides a second method to determine κ. Also, unlike C_2, D_2 does not depend on Reynolds number provided that the log-law constants are independent of Reynolds number.

In figure 9(*a*) we plot the variation of the friction factor with Reynolds number. The error bars represent the total uncertainty in the measurement ($\pm 1.1\%$ of the friction factor). Also shown is the formula proposed by Blasius (1913),

$$\lambda = 0.3164/Re^{0.25} \tag{32}$$

which is considered accurate for $Re < 100\times10^3$, but departs significantly from experimental data and the formula proposed by Prandtl at higher Reynolds numbers. The data are within $\pm 1\%$ of (32) for $Re < 75\times10^3$ and within $\pm 2\%$ at $Re = 98\times10^3$, and within $\pm 2\%$ of the relationship proposed by Prandtl for Reynolds numbers less than 2×10^6. For Reynolds numbers above 2×10^6, the friction factor is larger than that given by Prandtl's formula by an amount which increases with Reynolds number up to a maximum difference of 5.5% at $Re = 35\times10^6$. The difference between Prandtl's formula and our data is significantly larger than the estimated uncertainty of our measurements.

For further comparison with Prandtl's formula, in figure 9(*b*) we plot the friction factor results with the ordinate and abscissa implied by (25). Here the error bars represent the uncertainty in the ordinate, $\pm 0.55\%$. Inspection of figure 9(*b*) indicates

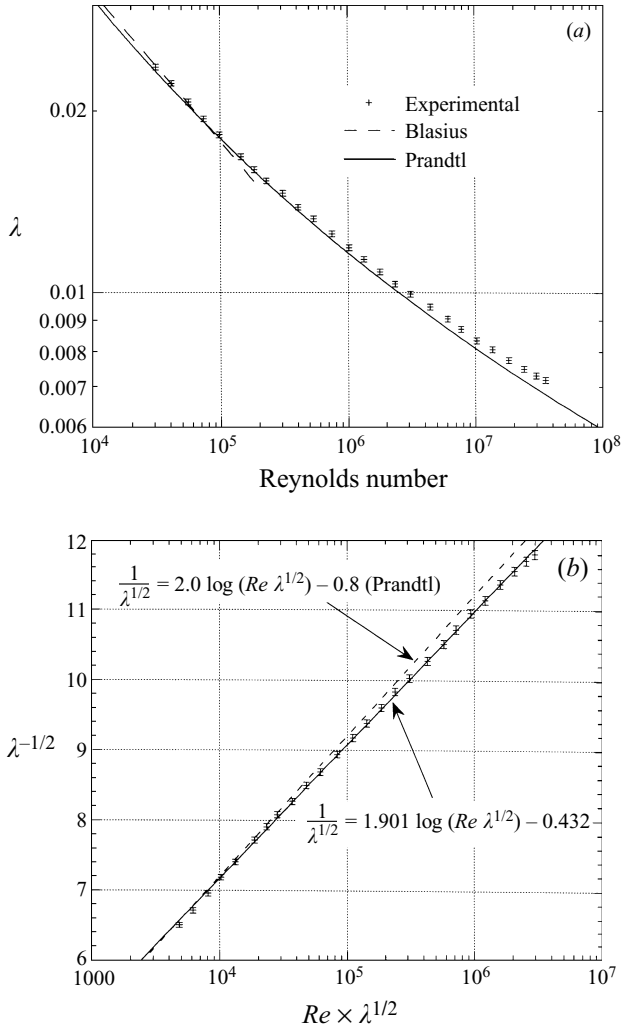

FIGURE 9. A comparison between our friction factor data with the relations proposed by (*a*) Prandtl and Blasius, (*b*) by Prandtl.

that the constants chosen by Prandtl do not accurately represent our data. A least-squares approximation (no weighting) was used with our data to determine new values for the coefficient in (25). When all Reynolds numbers are used in the analysis (Case 1 in table 3), the new values for the constants are 1.901 and -0.432. The agreement between this new curve and the data is satisfactory (see figure 9*b*), but more accurate relationships can be found as follows.

As discussed earlier, it seems reasonable to disregard the data below $\sim 100 \times 10^3$ when determining the coefficients in (25). Also, there may be a slight roughness effect at the very highest Reynolds number. Therefore, the coefficients in (25) were determined using $98 \times 10^3 \leqslant Re \leqslant 30 \times 10^6$ (Case 4 in table 3). For comparison with this Reynolds number range, the analysis was repeated for the different ranges given in table 3, where R_c is the correlation coefficient. The results from a least-squares approximation of Nikuradse's friction factor data are also given for two different ranges of Reynolds numbers. The coefficients found from Nikuradse's data for $3.1 \times 10^3 < Re < 3.2 \times 10^6$ are the same as those determined by Prandtl. The values of

Case number	Reynolds number range	C_1	C_2	R_c	κ
1	31×10^3–35×10^6	1.901	−0.432	0.99979	0.428
2	98×10^3–35×10^6	1.877	−0.298	0.99987	0.434
3	140×10^3–35×10^6	1.872	−0.270	0.99987	0.435
4	98×10^3–30×10^6	1.884	−0.331	0.99991	0.432
5	98×10^3–24×10^6	1.889	−0.358	0.99992	0.431
Nikuradse	3.1×10^3–3.2×10^6	2.00	−0.81	0.99875	0.407
Nikuradse	100×10^3–3.2×10^6	1.95	−0.55	0.99693	0.417

TABLE 3. Coefficients for equation (25)

the correlation coefficient for Cases 1–5 are all very close to 1 which indicates that functional form of (25) is in excellent agreement with the trends in the data. For Cases 2–5, the variation of C_1 and κ is small ($\pm0.5\%$ of the average value), but the variation of C_2 is large ($\pm14\%$ of the average value). The large variation in C_2 may be expected since the second term in (25) is a small fraction (2% to 4%) of the first term for all Reynolds numbers above 100×10^3.

An interesting result from table 3 is that $0.428\leqslant\kappa\leqslant0.435$ which is considerably larger than the values determined by other investigators including Nikuradse (1930) ($\kappa=0.40$), Coles (1955) ($\kappa=0.41$), Patel (1965) ($\kappa=0.42$), and Brederode & Bradshaw (1974) ($\kappa=0.41$). This observation will be discussed in the next section.

To investigate the friction factor relationship further, we define Θ given by

$$\Theta=\lambda[C_1\log(Re\,\lambda^{1/2})+C_2]^2, \tag{33}$$

where Θ is a measure of the 'goodness' of the curve fit. If the correlation coefficient equals 1, then $\Theta=1$, independent of Reynolds number. The uncertainty in Θ is approximately equal to the uncertainty in the friction factor. Therefore, if we choose C_1 and C_2 correctly, then all friction factor data that follow the relationship given by (25) should fall within $0.989<\Theta<1.011$.

If we neglect the data for $Re<98\times10^3$ and $Re=35\times10^6$ (Case 4 in table 3), the variation of Θ with Reynolds number is shown in figure 10(*a*). The upward trend of Θ at the very highest Reynolds numbers may well reflect the first influence or roughness on the results, although the agreement is still within the uncertainty of the data. The upward trend at the lower Reynolds numbers can be attributed to the Reynolds number dependence of the near-wall velocity profile.

To further investigate the low Reynolds number trend observed in figure 10(*a*), we need to take into account the Reynolds number dependence of the coefficient C_4. If we assume that the near-wall velocity profile can be accurately represented by the relation proposed by Spalding (1961), then C_4 is proportional to the difference between the log law and Spalding's relation averaged across the radius of the pipe (and is only significant for $y^+<50$). The difference was found using $\kappa=0.436$ and $B=6.13$. Since this term is a small correction to (25) it is not sensitive to the exact values of the constants. This analysis was incorporated into (25) and the friction data were reanalysed for the cases given in table 3. For this purpose, (25) was re-written as

$$\frac{1}{\lambda^{1/2}}=C_1\log(Re\,\lambda^{1/2})+C_2+C_4-\frac{233}{(Re\,\lambda^{1/2})^{0.90}}, \tag{34}$$

where

$$C_2+C_4=\frac{B}{2\sqrt2}-\frac{1}{\kappa}\left[\frac{\log(4\sqrt2)}{2\sqrt2\log(\mathrm{e})}+\frac{3}{4\sqrt2}\right]+C_3 \tag{35}$$

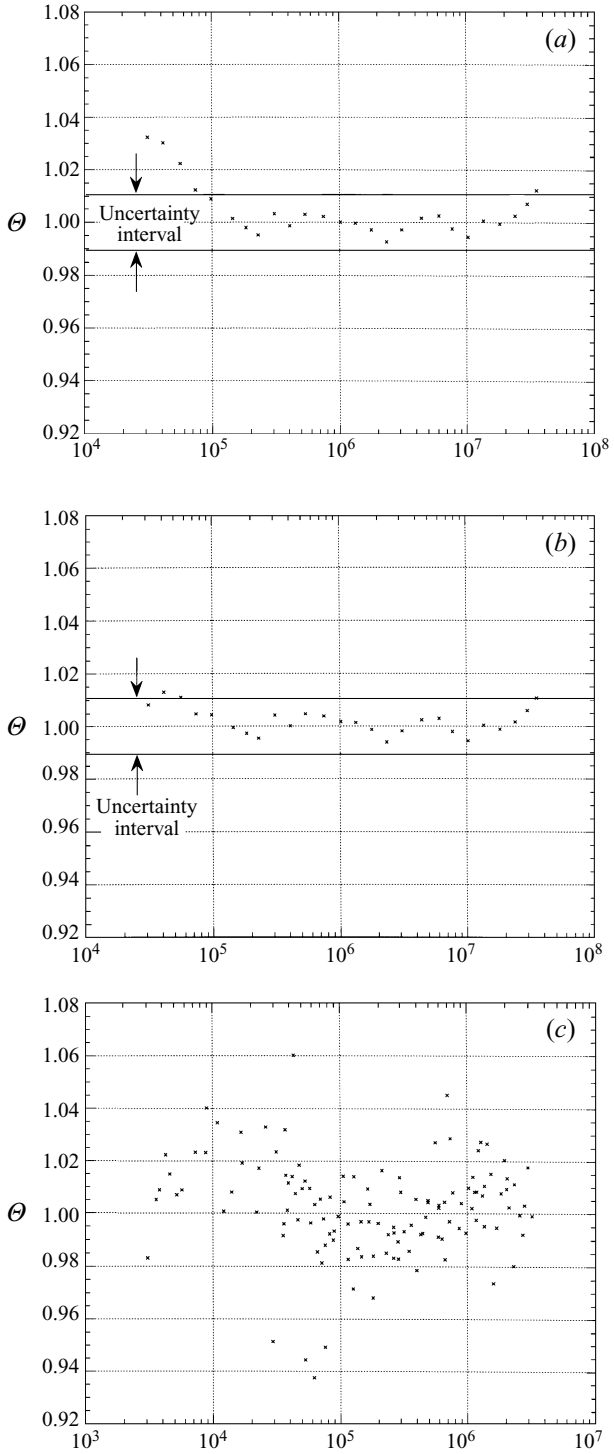

FIGURE 10. The friction factor ratio (equation (33)) as a function of Reynolds number for the coefficients given in (*a*) Case 4 of table 3, (*b*) Case 4 of table 4, (*c*) for the coefficients used by Prandtl (the data shown in (*c*) are from Nikuradse 1932).

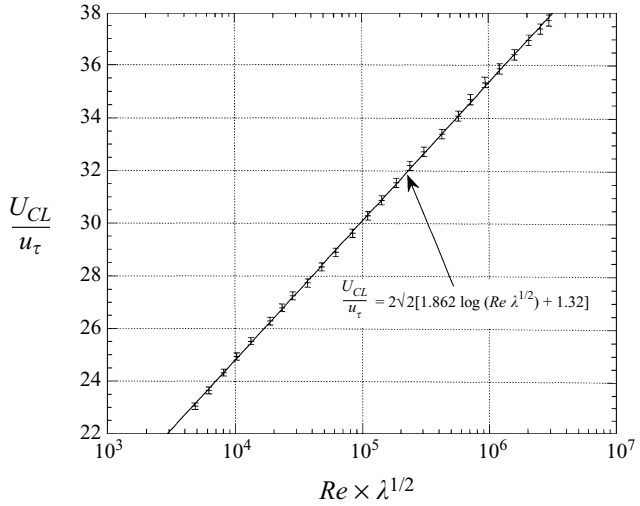

FIGURE 11. The variation of centreline velocity with Reynolds number.

Case number	Reynolds number range	C_1	C_2+C_4	R_c	κ
1	31×10^3–35×10^6	1.870	−0.266	0.99991	0.435
2	98×10^3–35×10^6	1.863	−0.212	0.99989	0.437
3	140×10^3–35×10^6	1.860	−0.198	0.99988	0.438
4	98×10^3–30×10^6	1.869	−0.241	0.99992	0.436
5	98×10^3–24×10^6	1.873	−0.263	0.99993	0.435

TABLE 4. Coefficients for equation (34)

and is believed to be independent of Reynolds number if a log law exists. Note that there were only two free parameters in the least-squares approximation, C_1 and C_2+C_4, and the data were not weighted. The results of this analysis are shown in table 4.

Comparison between the results given in tables 3 and 4 reveals that for the results derived using (34), the correlation coefficient is closer to 1 and the variation of C_1 and κ from case to case is less (±0.002 for κ). Also, the value for κ for each case has increased by approximately 0.004. In figure 10(*b*), we show the variation of Θ with Reynolds number for the coefficients given in table 4 for Case 4. For the entire Reynolds number range, Θ is within $\pm1.3\%$ of 1 which is close to the uncertainty in λ ($\pm1.1\%$). The agreement with data at low Reynolds numbers is remarkable in the light of the crude near-wall correction term.

We now can postulate two new friction factor relationships, one which neglects the Reynolds number dependence of the velocity profile near the wall, and one which accounts for this dependence. For Reynolds number between 100×10^3 and 35×10^6, a new friction factor relation is proposed which has the same functional form as the one proposed by Prandtl but has different values for the coefficients. This new relation is given by

$$\frac{1}{\lambda^{1/2}} = 1.884\log(Re\,\lambda^{1/2}) - 0.331 \tag{36}$$

Case number	Reynolds number range	D_1	D_2	R_c	κ
1	31×10^3–35×10^6	1.862	1.321	0.99987	0.437
2	98×10^3–35×10^6	1.858	1.347	0.99982	0.438
3	140×10^3–35×10^6	1.860	1.335	0.99979	0.438
4	98×10^3–30×10^6	1.863	1.323	0.99982	0.437
5	98×10^3–24×10^6	1.868	1.299	0.99982	0.436
Nikuradse	3.1×10^3–3.2×10^6	1.96	0.85	0.99810	0.415
Nikuradse	100×10^3–3.2×10^6	1.85	1.37	0.99560	0.440

TABLE 5. Coefficients for equation (29)

(Case 4 in table 3). This relation is believed to predict the friction factor in a smooth pipe to better than $\pm1.2\,\%$ for Reynolds numbers between 98×10^3 and 35×10^6. The fit at lower Reynolds numbers is somewhat poorer because the near-wall region occupies a significant portion of the radius for $Re<98\times10^3$.

The coefficients in (36) should be preferred over the ones adopted by Prandtl because the data used to determine these are considerably more accurate than the data used by Prandtl (Nikuradse 1932). To illustrate this point, we plot Θ as a function of Reynolds number for Nikuradse's data in figure 10(*c*). Here the values of C_1 and C_2 used to calculate Θ were the ones used by Prandtl (2.0, -0.8). (When all of Nikuradse's data are used in this analysis, $C_1=2.000$.) The standard deviation in these data is at least a factor of three larger than for our data. Also, in determining C_1 and C_2, Prandtl used all of Nikuradse's friction factor data, to Reynolds numbers as low as 3.1×10^3 where it is doubtful a log law exists (see Patel & Head 1969). If we neglect Nikuradse's data for $Re<100\times10^3$, then $C_1=1.95$, which is closer to the value we obtained.

For a wider range of Reynolds numbers, a new friction factor relation is proposed which is similar to Prandtl's relation, but with new coefficients and an additional term to account for the form of the near-wall velocity profile. The new relation is given by

$$\frac{1}{\lambda^{1/2}}=1.869\log(Re\,\lambda^{1/2})-0.241-\frac{233}{(Re\,\lambda^{1/2})^{0.90}} \tag{37}$$

(Case 4 in table 4). This relation is believed to predict the friction factor in smooth pipes to better than $\pm1.3\,\%$ for Reynolds numbers between 10×10^3 and 35×10^6. Equation (37) represents the subtleties of the mean velocity profile better than (36) and therefore should be preferred.

The analysis performed with the friction factor data was repeated with the U_{CL}/u_τ data. In figure 11, we plot U_{CL}/u_τ as a function of $\log(Re\,\lambda^{1/2})$. The error bars on the data represent the uncertainty in our measurement of U_{CL}/u_τ ($\pm0.55\,\%$). Also shown in figure 11 is a curve-fit of the data determined by a least-squares approximation of (29). For the curve shown, all data were used to determine the coefficients (Case 1 in table 5). For comparison with the friction factor data, the same Reynolds number ranges were analysed and the coefficients from the least-squares approximation are given in table 5. Also given are the coefficients from an analysis of Nikuradse's data for two different Reynolds number ranges. The coefficients determined from our data display smaller variations than the corresponding friction factor data shown in tables 3 and 4. This can be partly attributed to the fact that the coefficients in (29) are independent of Reynolds number if the log-law constants are independent of Reynolds number. The value of κ for Cases 2–5 in table 5 are within 0.001 of the corresponding

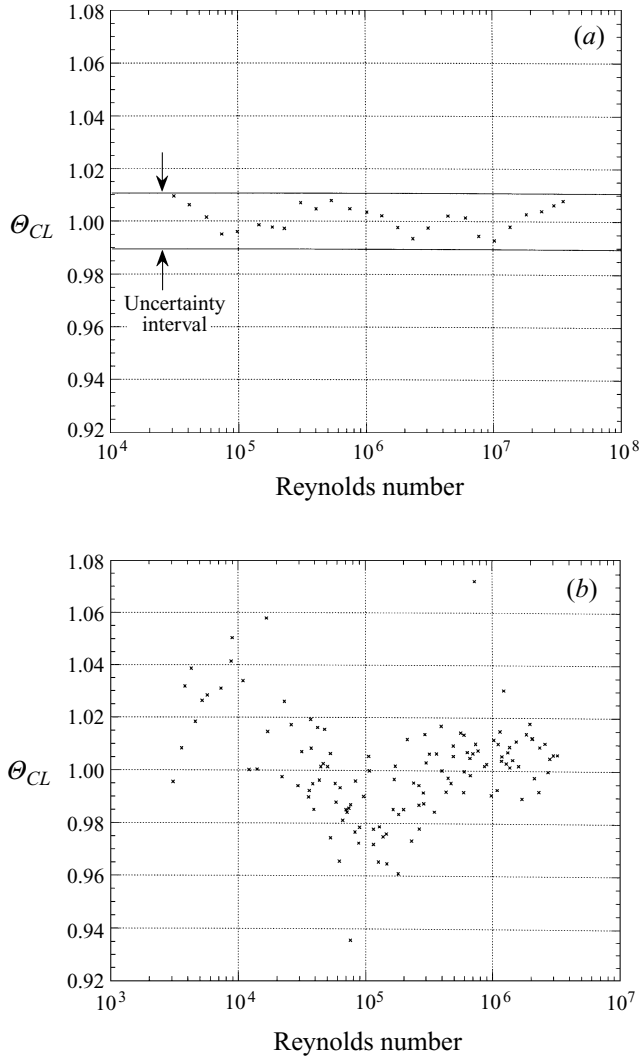

FIGURE 12. The variation of the resistance coefficient ratio (equation (38)) with Reynolds number for the coefficients given in (*a*) Case 4 of table 5, and (*b*) for the coefficients determined from the data measured by Nikuradse (1932).

values in table 4. A review of tables 4 and 5 reveals that κ has a consistent value of 0.436 ± 0.002.

For comparison with Θ, we define Θ_{CL} as

$$\Theta_{CL} = 8\left(\frac{u_\tau}{U_{CL}}\right)^2 [D_1 \log(Re\,\lambda^{1/2}) + D_2]^2, \tag{38}$$

where Θ_{CL} should have the same uncertainty as Θ (equation (33)). In figure 12(*a*) we show the variation of Θ_{CL} with Reynolds number using the coefficients determined for Case 4 in table 5. The value of Θ_{CL} appears to be randomly distributed within $\pm 0.9\,\%$ of 1 which is less than the uncertainty of $(U_{CL}/u_\tau)^2$ ($\pm 1.1\,\%$). Using the coefficients in Case 4, a relationship for U_{CL}/u_τ can be written as

$$U_{CL}/u_\tau = 5.269 \log(Re\,\lambda^{1/2}) + 3.742. \tag{39}$$

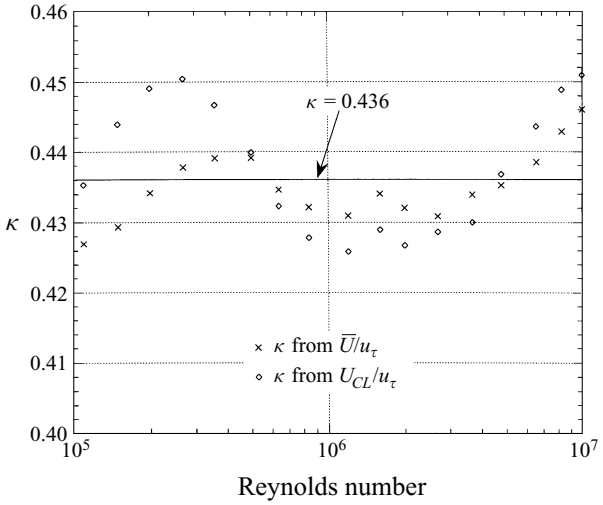

FIGURE 13. The variation of κ for successive Reynolds number groupings.

Series number	Reynolds number range	Mean Reynolds number
1	31×10^3–410×10^3	110×10^3
2	41×10^3–540×10^3	150×10^3
3	56×10^3–750×10^3	200×10^3
4	74×10^3–1.0×10^6	270×10^3
5	98×10^3–1.3×10^6	360×10^3
6	140×10^3–1.8×10^6	500×10^3
7	180×10^3–2.3×10^6	640×10^3
8	230×10^3–3.1×10^6	840×10^3
9	310×10^3–4.4×10^6	1.2×10^6
10	410×10^3–6.1×10^6	1.6×10^6
11	540×10^3–7.7×10^6	2.0×10^6
12	750×10^3–10×10^6	2.7×10^6
13	1.0×10^6–14×10^6	3.7×10^6
14	1.3×10^6–18×10^6	4.8×10^6
15	1.8×10^6–24×10^6	6.6×10^6
16	2.3×10^6–30×10^6	8.3×10^6
17	3.1×10^6–35×10^6	10×10^6

TABLE 6. Reynolds number range of each series

Equation (39) should predict U_{CL}/u_τ to within $\pm0.55\%$ for Reynolds numbers between 31×10^3 and 35×10^6. By comparison with the friction factor data, we may expect that the lower limit of (39) can be extended to 10×10^3 with no loss of accuracy.

A similar analysis was performed using Nikuradse's data and the results are given in table 5 and shown in figure 12(*b*). The value of κ in table 5 is consistent with the value obtained from Nikuradse's friction factor data when the full Reynolds number range is analysed (e.g. $\kappa = 0.407$ from the friction factor data and $\kappa = 0.415$ from the centreline velocity data), but if we neglect the data for $Re < 100\times10^3$, then we find $\kappa = 0.440$, which is very close to the value obtained using our new data, but different than the value obtained from Nikuradse's friction factor data (0.417). The

inconsistency between Nikuradse's friction factor and centreline velocity data must call into question either the accuracy of his measurements or the existence of a log law. The validity of the log law will be discussed in the next section. In figure 12(*b*), we show Θ_{CL} as a function of Reynolds number from the analysis using Nikuradse's entire data set. Similar to the friction factor data, the standard deviation in these data is at least a factor of three larger than for our data.

To this point, we have assumed that κ is independent of Reynolds number. In fact, the data presented in this section can also be used to examine the Reynolds number dependence of κ by determining C_1 and D_1 over a limited range of Reynolds numbers. Since any Reynolds number dependence should be weak, it seems reasonable to analyse series consisting of 10 consecutive Reynolds numbers which cover an order of magnitude in R^+ (and $Re\,\lambda^{1/2}$). The ranges of Reynolds numbers analysed for each series are given in table 6 along with a mean Reynolds number for each series. The mean Reynolds number corresponds to the mean of the log of the maximum and minimum Reynolds number in a series. For each series, κ was calculated from a least-squares approximation using (25) and (29). The results are shown in figure 13.

The values of κ for most of the series are between 0.425 and 0.450 (0.438 ± 0.013). The scatter in κ derived from the U_{CL}/u_τ data is larger than the scatter in κ derived from the friction factor data. There appears to be a similar trend in both data sets in that κ has a minimum value between Series 9 and Series 11 (mean Reynolds number between 1.2×10^6 and 2.0×10^6). Although $\kappa = 0.436$ is in reasonable agreement with the U_{CL}/u_τ data and friction factor data over the entire range of Reynolds numbers, there may be a Reynolds number dependence over a limited range of Reynolds numbers. To investigate the dependence further, we need to examine the mean velocity profiles.

7. Velocity profile results: inner scaling

The velocity profiles normalized using inner scaling variables are shown in figure 14 for 13 different Reynolds numbers between 31×10^3 and 35×10^6. The profiles at intermediate Reynolds numbers were omitted for clarity, but the trends observed at intermediate Reynolds numbers are consistent with the ones shown. All profiles in figure 14 do not extend to $y^+ \approx 7$, but each covers a range of y^+ which is approximately two orders of magnitude. Inspection of figure 14 indicates that the velocity profiles for different Reynolds numbers are in good agreement where they overlap in y^+. In the core region, the scaling used in this graph is no longer appropriate, and the profiles should not collapse onto a single curve. Also shown in figure 14 is a log law with $\kappa = 0.41$ and $B = 5.2$. If the data in the core region and near-wall region ($y^+ < 50$) are neglected, then there appears to be a range of y^+ where this log law exists. However, at the higher Reynolds numbers, where the existence of the log law is most likely, the agreement between the log law shown and the data is poor.

These inconsistencies can be resolved by adjusting the limits of the log law from the conventional limits of $50 < y^+ < 0.15R^+$ to more restrictive limits. To establish these limits, we define Ψ as

$$\Psi = U^+ - \frac{1}{\kappa}\ln y^+, \tag{40}$$

where Ψ should equal B in the logarithmic region. If a log law exists, then by plotting Ψ versus the wall-normal positions a horizontal line should be evident provided that κ was chosen correctly. If the wall-normal positions are scaled by inner layer variables,

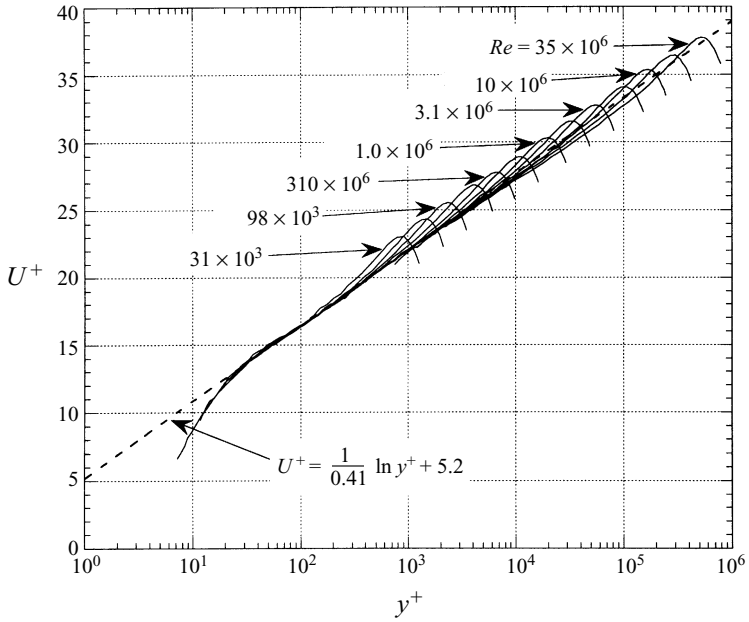

FIGURE 14. A comparison of the velocity profiles normalized using inner scaling variables for 13 different Reynolds numbers between 31×10^3 and 35×10^6.

then the near-wall limit of the log law (M_i) should become apparent. If the wall-normal positions are scaled by outer layer variables, then the core limit of the log law (M_o) should become apparent.

The value of Ψ was calculated using the value of κ determined from the friction factor and centreline velocity data ($\kappa = 0.436$). Data for $y/R < 0.01$ were neglected in this analysis due to the large uncertainty in position and the data at the very highest Reynolds number were neglected due to the possibility of roughness effects (see figure 8). To determine the inner limit, the Ψ data at each y^+ location were averaged. Data for $y/R > M_o$ were neglected to prevent data in the core region, where $\Psi > B$, from increasing the average at a given y^+. To determine the outer limit, the Ψ data at each y/R location were averaged. Data for $y^+ < M_i$ were neglected to prevent data in the near-wall region, where $\Psi < B$, from reducing the average at a given y/R. The limits were adjusted until a consistent value of Ψ was obtained for some intermediate region given by $M_i \nu/u_\tau < y < M_o R$.

The results are shown in figure 15(a, b). The error bars shown correspond to the standard error (95% confidence interval) at a given position. These error bars are considerably smaller than the uncertainty in B for a single Reynolds number (± 0.12) (see figure 8). The large uncertainty in figure 8 is due primarily to the uncertainty in u_τ which has a fixed value at a given Reynolds number. When an average is taken over multiple Reynolds numbers, the random error in u_τ tends to cancel providing us with a more accurate method to determine B. The values of Ψ shown in figure 15(a, b) are averages for data at six to seventeen Reynolds numbers. Inspection of figures 15(a) and 15(b) shows that for $600\nu/u_\tau < y < 0.07R$ ($600 < y^+ < 0.07R^+$), Ψ has a constant value of 6.15 in both figures.

Our proposed log-law limits are more restrictive than the commonly accepted limits of $50\nu/u_\tau < y < 0.15R$ but are consistent with Millikan's proposal in that a logarithmic overlap region can only exist for ν/u_τ y R or 1 y^+ R^+. These limits are also

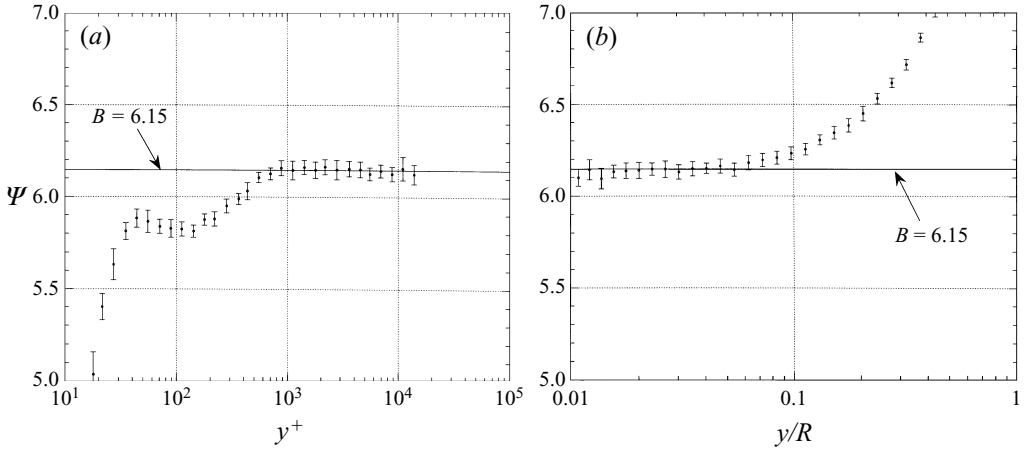

FIGURE 15. The difference between the velocity profile and the log law as a function of wall-normal position for $\kappa = 0.436$. The value of Ψ was averaged over multiple Reynolds numbers. In (*a*) the wall-normal positions are normalized using inner scaling variables, and in (*b*) outer scaling variables.

similar to the ones determined by George *et al.* (1997) ($300 < y^+ < 0.1R^+$) from a simplified turbulence model. Accepting our proposed limits, a log law cannot exist for $R^+ < 600/0.07 = 9 \times 10^3$ which corresponds to a pipe Reynolds number of 400×10^3. It is doubtful that other experiments could have defined these limits since to observe a log law over an order of magnitude in y^+ requires data at a Reynolds number of 5×10^6 which has only been obtained here and in the experiment by Dickinson (1975).

Critics of the log law often point to the Reynolds number dependence of the peak in the Reynolds shear stress, which may occur in the log region, as evidence against the existence of a log region. This criticism is based on the belief that if the log region is truly an inertial region then the turbulence statistics must be independent of viscous effects. We argue that the limits we propose resolve this apparent contradiction. An equation for the Reynolds shear stress in the log region can be derived from the streamwise momentum equation as

$$-\overline{uv}^+ = 1 - \frac{y^+}{R^+} - \frac{1}{\kappa y^+}, \tag{41}$$

where $-\overline{uv}^+$ is the Reynolds shear stress normalized by u_τ. Equation (41) can be used to show that the peak in $-\overline{uv}^+$ occurs at

$$y_p^+ = \left(\frac{1}{\kappa} R^+\right)^{1/2}. \tag{42}$$

If a log law is not observed until $R^+ \approx 9 \times 10^3$, then the location of the peak is inconsequential since $-\overline{uv}^+ \approx 1$ and viscous effects are negligible. This is not the case if we use the conventional limits for the log law since a log law would then exist at $R^+ \approx 50/0.15 \approx 330$ and

$$-\overline{uv}^+ = 1 - \left(\frac{4}{\kappa R^+}\right)^{1/2} = 0.83 \tag{43}$$

if we let $\kappa = 0.41$. The proposed log-law limits are consistent with the streamwise

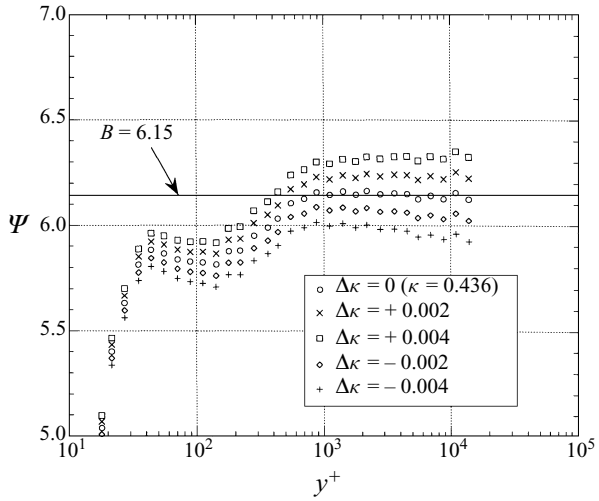

FIGURE 16. The difference between the velocity profile and the log law as a function of wall-normal position for different values of κ. The value of Ψ was averaged over multiple Reynolds numbers.

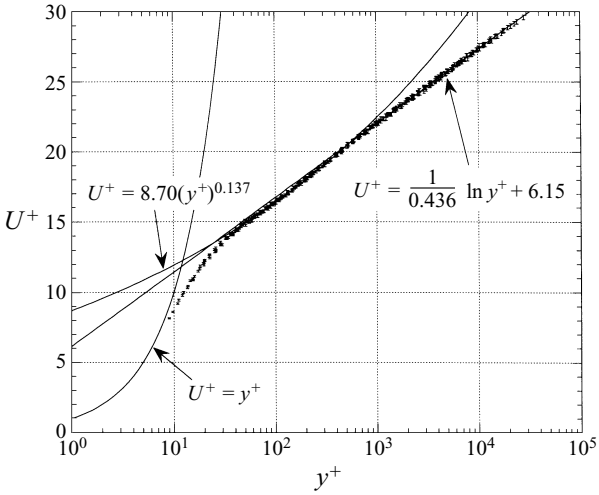

FIGURE 17. A linear–log plot of the velocity profile data within $0.07R^+$ of the wall normalized using inner scaling variables for 26 different Reynolds numbers from 31×10^3 to 35×10^6.

momentum equation while the previously accepted limits appear to create a contradiction between the equations of motion and the overlap argument used to derive the log law.

The new log-law limits were used to determine B for each Reynolds number. The results are shown in figure 8 which is described in §5. The additive constant has an average value of 6.15 with a standard error of ± 0.02 when the highest Reynolds number is neglected. No Reynolds number dependence is apparent except at the highest Reynolds number and, as pointed out in §5, this may be caused by roughness.

So far we have assumed that $\kappa = 0.436$. In figure 16 we show Ψ for $\kappa = 0.436 \pm 0.002$ and ± 0.004. The data for $\kappa = 0.436$ and $\kappa = 0.438$ form a horizontal line for $y^+ > 600$. For $\kappa = 0.438$ the nominal value of B is 6.23. For the other values of κ, Ψ has either

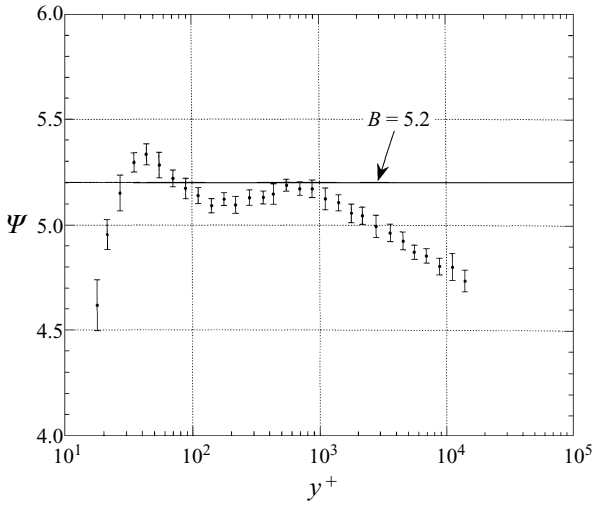

FIGURE 18. The difference between the velocity profile and the log law as a function of wall-normal position for $\kappa = 0.41$. The value of Ψ was averaged over multiple Reynolds numbers.

a positive or negative slope for $y^+ > 600$. It appears that $\kappa = 0.436 \pm 0.002$ is consistent with the velocity profile data as well as the friction factor and resistance coefficient data (U_{CL}/u_τ), and that $B = 6.15 \pm 0.08$ is consistent with the velocity profile data. The uncertainty in B is due entirely to the uncertainty in κ. For a fixed value of κ, the standard error in B is ± 0.02.

For $600 < y^+ < 0.07R^+$, the U^+ data are well represented by a log law given by

$$U^+ = \frac{1}{0.436} \ln y^+ + 6.15. \tag{44}$$

A comparison between (44) and the data is shown in figure 17. The data measured at the maximum Reynolds number were neglected in this figure and the size of the symbols is equal to the uncertainty in U^+ ($\pm 0.57\%$). The U^+ data are within $\pm 0.58\%$ ($= 2 \times$ standard deviation) of the log law shown for $600 < y^+ < 0.07R^+$. The standard deviation is approximately equivalent to the uncertainty in U^+, indicating that the log law is in excellent agreement with the data.

We have presented evidence that the correct values of κ and B are 0.436 and 6.15 which are significantly different than the widely accepted values of 0.41 and 5.2 (see Brederode & Bradshaw 1974, for example). To investigate this discrepancy, we determined Ψ as a function of y^+ for $\kappa = 0.41$ using the same analysis used to produce figures 15(*a*) and 16. The results are shown in figure 18. Also shown is the standard error of Ψ (95% confidence interval). The value of Ψ is within ± 0.1 of $B = 5.2$ for $50 < y^+ < 1 \times 10^3$. The variation of Ψ is considerably larger than the standard error, indicating a log law with this value of κ is not in good agreement with these data. If we assume that the outer limit of the log law is given by the conventional value of $y \approx 0.15R$, then this range of y^+ corresponds to $300 < R^+ < 7 \times 10^3$ or $9 \times 10^3 < Re < 300 \times 10^3$ which is the range of Reynolds numbers studied in most previous investigations. We argue that previous investigators have assumed the existence of a log law at these Reynolds numbers. Discrepancies between log-law constants have been attributed to a Reynolds number dependence of the constants (incomplete similarity) or experimental error, but it appears that these discrepancies are due to the fact that the scaling in this region is not logarithmic.

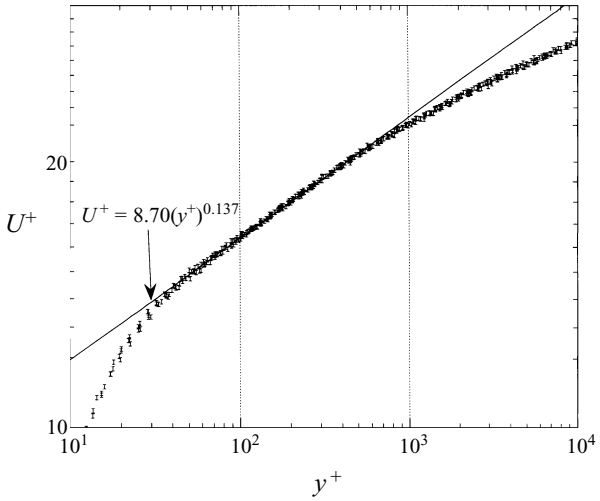

FIGURE 19. A log–log plot of the velocity profile data within $0.07R^+$ of the all normalized using inner scaling variables for 26 different Reynolds numbers from 31×10^3 to 35×10^6.

We believe that this region, which is closer to the wall than the log region and further from the wall than the linear region, is better described by a power law than a log law (Zagarola & Smits 1997). The power law is shown in figure 17. The local value of κ can be evaluated from the slope of the power law using

$$\kappa = \left(y^+ \frac{\mathrm{d}U^+}{\mathrm{d}y^+} \right)^{-1}. \tag{45}$$

The value of κ varies from 0.49 to 0.36 for $50 < y^+ < 500$ which is consistent with the variation observed by many previous investigators (Hinze 1964), and helps explain why previous investigators have noted a Reynolds number dependence of the log-law constants.

Finding the empirical constants and the limits of a power law are more difficult than for the log law since neither of the constants is readily determined from the friction factor data. The inner limit of the power law should scale on inner layer variables, but the outer limit may scale on inner or outer layer variables depending on whether the Reynolds number is large enough for a logarithmic overlap region to exist. From inspection of figure 17, the inner limit of the power law appears to be at $y^+ \approx 50$ or 60. At Reynolds numbers sufficiently large for a log law to exist ($R^+ \approx 9 \times 10^3$), we may expect that the outer limit of the power law region is equivalent to the inner limit of the log law ($y^+ \approx 600$). At lower Reynolds numbers, we expect viscous effects and the power law scaling to extend beyond where the outer limit of the log law is located ($y^+ \approx 0.07R^+$). We can take $y^+ = 0.15R^+$ as a first approximation since it is the conventional outer limit of the log law.

The empirical constants in the power law were determined using a least-squares approximation for the region given by $60 < y^+ < 500$ or $0.15R^+$. The data for $500 < y^+ < 600$ are inconsistent with the power law scaling, and we believe that this region is a transition region between the power law and log law. In figure 19 we plot the U^+ data in log–log coordinates in order to emphasize the power law dependence. The power law is given by

$$U^+ = 8.70(y^+)^{0.137}. \tag{46}$$

The U^+ data are within $\pm 0.72\,\%$ ($= 2 \times$ standard deviation) of (46) for $60 < y^+ < 500$

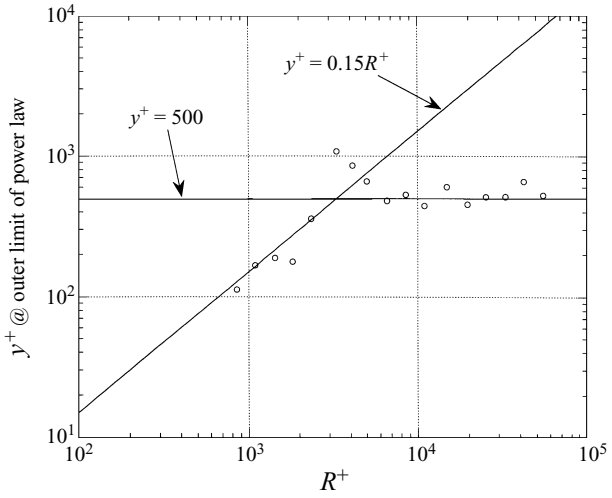

FIGURE 20. The outer limit of the power law region as a function of Reynolds number.

or $0.15R^+$ which is commensurate with the uncertainty in U^+ ($\pm 0.57\%$). The multiplicative constant and the exponent in (46) are very close to the values (8.74, $1/7 = 0.143$) that Prandtl derived (see Durand 1943) from the Blasius friction factor relation (equation (32)) using the assumption $\bar{U} = 0.8U_{CL}$, and which Nikuradse (1932) showed were in good agreement with his low Reynolds number data.

In figure 20, we show the outer limit of the power law as a function of R^+. The outer limit was determined as the point where the uncertainty intervals of the U^+ data no longer overlap (46). The outer limit appears to depend on Reynolds number for $R^+ < 6 \times 10^3$, and above this value, it appears to be independent of Reynolds number and constant at approximately $y^+ \approx 500$. For $R^+ < 2.7 \times 10^3$, the outer limit is in reasonable agreement with $y^+ = 0.15R^+$. For $2.7 \times 10^3 < R^+ < 5 \times 10^3$, the power law appears to extend considerably further into the outer region ($y \approx 0.3R$ to $0.6R$) than for the other Reynolds numbers. We believe that this anomaly occurs because the slope of the velocity profile at the outer limit of the power law, which depends on R^+, coincides with the slope near the inner limit of the outer region at these Reynolds numbers. We do not believe that the extension of the power law this far from the wall is indicative of a viscous dependence.

8. A new scaling argument for the inner region

The existence of a power law implies that viscosity is still an important parameter for $y^+ < 500$. The viscous dependence suggests that this region is part of the inner region, but since the Reynolds number must be quite large for this region to exist, it could also be an overlap region exhibiting incomplete similarity (Zagarola & Smits 1997). The lowest Reynolds number where the power law exists is $Re \approx 13 \times 10^3$ ($R^+ \approx 400$). The existence of an overlap region at this Reynolds number is supported by the investigation by Patel & Head (1969) in which they observed an overlap region for $Re > 10^3$. They concluded that the overlap region was logarithmic, but it is doubtful that the scaling could be determined at such low Reynolds numbers.

It could also be argued that at sufficiently high Reynolds numbers the power law becomes the log law. This scenario is consistent with Prandtl's speculation (see Durand

1943), but it does not appear to be the case. The highest Reynolds number where the velocity profile exhibits a power law dependence is $Re = 2.3 \times 10^6$ ($R^+ = 42 \times 10^3$), and the lowest Reynolds number that exhibits a log law dependence is $Re = 410 \times 10^3$ ($R^+ = 8.5 \times 10^3$), so there are surveys at seven different Reynolds numbers that exhibit both a log and power law region. Note that Prandtl's proposal would be consistent with our observations if the Reynolds number dependence in Prandtl's argument was replaced with a y^+ dependence.

Here we postulate a reason for the existence of two overlap regions, one which scales as a power law and one which scales as a log law. In §1, the scaling laws for the mean velocity profile were presented in the form originally proposed by Prandtl (near-wall region), von Kármán (outer region) and Millikan (overlap region). The inner scaling law is repeated here in its original form:

$$U^+ = f(y^+). \tag{47}$$

The outer scaling law can be written in an alternative form as

$$\frac{U_{CL} - U}{u_o} = g(\eta), \tag{48}$$

where u_o is the velocity scale in the outer region.

Equations (47) and (48) are based on the assumption that R^+ is large enough for both regions to be independent of Reynolds number. If we assume that an intermediate region exists where both scaling laws are valid, then we can define two different matching conditions. By matching the velocity gradients given by (47) and (48), we find

$$y^+ f' = -\Lambda \eta g' \tag{49}$$

where the differentiation in (49) is with respect to the dependent variables and Λ is the ratio of the outer to inner velocity scales, u_o/u_τ. If $u_o = u_\tau$, then (49) is the same relation used by Millikan to derive the classical logarithmic overlap region.

Alternatively, if we simultaneously match the velocities and velocity gradients, the matching condition is

$$y^+ \frac{f'}{f} = -\frac{\eta g'}{(U_{CL}/u_o) - g}. \tag{50}$$

Equation (50) is the same relation used by George *et al.* (1996) with $u_o = U_{CL}$ to support their assertion that the overlap region in boundary layers is given by a power law at sufficiently high Reynolds numbers.

We argue that at low Reynolds number, but still high enough that an overlap region exists, Λ is a function of R^+. At these Reynolds numbers, (49) does not define an overlap region that is independent of R^+, but (50) does. From (50), the differential equation can be written in terms of inner scaling variables as

$$y^+ \frac{f'}{f} = \gamma, \tag{51}$$

where γ is an unknown but fixed constant. The fixed value of γ is a consequence of the assumption of Reynolds number independence of the inner and outer regions. Therefore, it is an asymptotic result that could be modified if the assumptions regarding the scaling of the inner and outer regions were relaxed or shown to be incorrect by experiment. Our observations provide no basis for this approach.

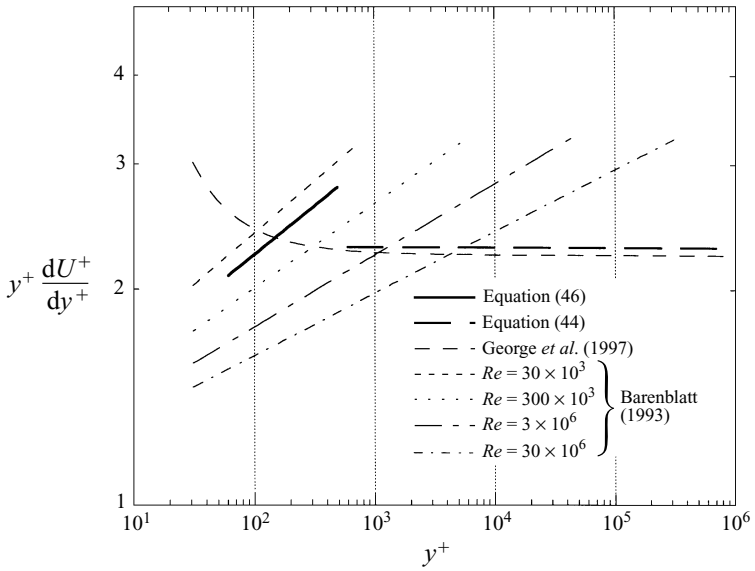

FIGURE 21. A comparison between overlap proposals.

Equation (51) can be integrated from the inner limit of this overlap region to some distance y^+ to give

$$U^+ = C_1(y^+)^\gamma, \tag{52}$$

where the constant C_1 should be independent of R^+ if the inner integration limit is independent of Reynolds number, and it appears to be (see figure 19). An equation equivalent to (51) can be written in terms of outer scaling variables. When integrated from the outer limit of the power law, the result is

$$\frac{U_{CL} - U}{u_o} = \frac{U_{CL}}{u_o} - C_2\,\eta^\gamma \tag{53}$$

or

$$\frac{U}{u_o} = C_2\,\eta^\gamma, \tag{54}$$

where C_2 appears to depend on Reynolds number since the outer limit of the power law scales on inner layer variables at high Reynolds numbers (see figure 20).

At sufficiently high Reynolds numbers, we argue that u_o/u_τ approaches a finite limit. For this case, (49) also gives an overlap region which is independent of Reynolds number. Equation (49) can be set equal to an empirical constant (typically $1/\kappa$) and integrated to give the classical log law which can be written in terms of both inner and outer scaling variables ((6) and (7)).

The transition from a power law to a log law can be interpreted as γ demonstrating a y^+ dependence (not a Reynolds number dependence specifically) over a relatively short interval in y^+. To illustrate this point, in figure 21 we plot $y^+\,\mathrm{d}U^+/\mathrm{d}y^+$ as a function of y^+ using log–log coordinates. If the functional dependence in the overlap region is a log law, then $y^+\,\mathrm{d}U^+/\mathrm{d}y^+$ is equal to a constant ($= 1/\kappa$, see (49)). If the functional dependence in the overlap region is a power law, then $\log(y^+\,\mathrm{d}U^+/\mathrm{d}y^+)$ is a linear function of $\log y^+$ with slope equal to γ. Figure 21 shows that the change from a power law to a log law occurs relatively abruptly in y^+.

Also shown in figure 21 are the recent overlap proposals by George *et al.* (1997) and

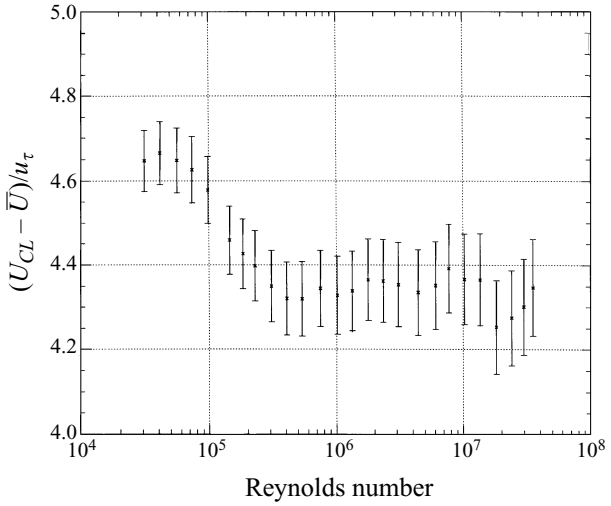

FIGURE 22. The difference between the average and centreline velocity as a function of Reynolds number.

Barenblatt (1993). Both proposals presume a smooth or gradual variation of the scaling in the overlap region. The proposal by George *et al.* presumes a smooth variation of $y^+ \mathrm{d}U^+/\mathrm{d}y^+$ with y^+. The proposal by Barenblatt presumes a smooth variation of C_1 and γ with Reynolds numbers. The variation of $y^+ \mathrm{d}U^+/\mathrm{d}y^+$ at four different Reynolds number is shown in figure 21. These proposals clearly differ in spirit from the proposal given here. Despite the abrupt change in scaling, we note that the entire overlap region in our model is still described only in terms of classic inner and outer scales. The functional dependence is observed to change, but the power-law and log-law regions should not be thought of as two separate overlap regions because they share the same scaling variables.

For our overlap proposal to be valid, u_o must be proportional to u_τ at high Reynolds number. From our analysis, it appears that a reasonable candidate for u_o is $U_{CL}-\bar{U}$, which is a true outer velocity scale, in contrast to u_τ, which is a velocity scale associated with the near-wall region which is 'impressed' on the outer region. Figure 22 shows the variation of $(U_{CL}-\bar{U})/u_\tau$ with Reynolds number. At Reynolds numbers less than $\sim 300\times10^3$, u_o/u_τ is a function of Reynolds number, but at high Reynolds numbers, u_o/u_τ is independent of Reynolds number (i.e. $u_o/u_\tau = \text{constant}$). For Reynolds numbers greater than 300×10^3, the error bounds for all data overlap a horizontal line at $(U_{CL}-\bar{U})/u_\tau = 4.34$. If $U_{CL}-\bar{U}$ is the correct outer velocity scale, then it should collapse the velocity profiles in the outer region for different Reynolds numbers onto a single curve. A comparison between the velocity profiles in the outer region scaled by $U_{CL}-\bar{U}$ and u_τ is given in §9.

9. Velocity profile results: Outer scaling

In figure 23(*a*, *b*) we plot the velocity profiles scaled by u_τ and $U_{CL}-\bar{U}$ for seven different Reynolds numbers between 31×10^3 and 35×10^6. When the velocity profiles are scaled by u_τ, the profiles do not collapse onto a single curve. The poor collapse is particularly evident for $0.07 < y/R < 0.30$ which is part of the overlap or core region depending on the Reynolds number. When using $U_{CL}-\bar{U}$ to scale the profiles (figure 23*b*), the collapse of the profiles is much improved for $y/R > 0.10$. For both scalings,

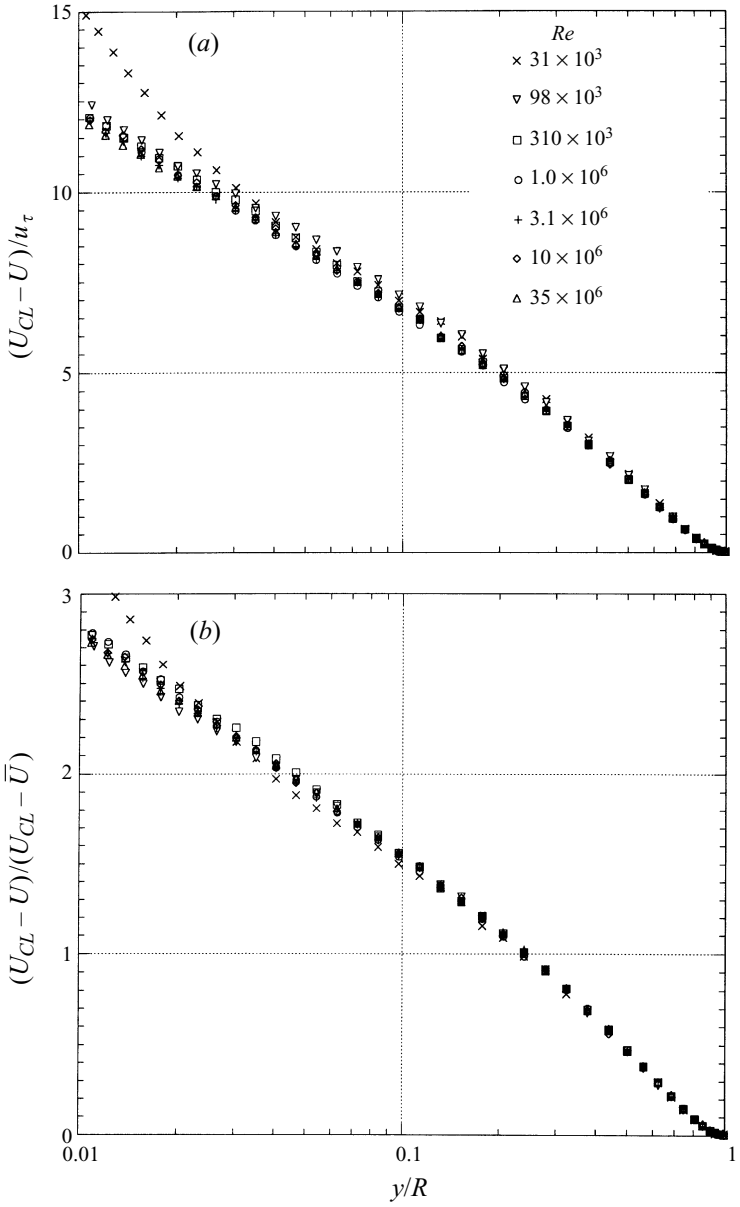

FIGURE 23. A comparison between the velocity profiles normalized by (*a*) u_τ and (*b*) $U_{CL}-\bar{U}$ for Reynolds numbers between 31×10^3 and 35×10^6.

the collapse in the overlap region is not very satisfactory. For low Reynolds numbers, this behaviour should be expected because an overlap region which is independent of Reynolds number (log law) does not exist for $Re < 400\times10^3$.

The difference between the velocity scales is more evident at low Reynolds numbers since at high Reynolds numbers the scales are proportional. Therefore, in figure 24(*a*, *b*) we plot the velocity profiles normalized by u_τ and $U_{CL}-\bar{U}$, respectively, for all Reynolds numbers investigated between 31×10^3 and 540×10^3. A comparison between the figures 24(*a*) and 24(*b*) indicates that the data scaled by $U_{CL}-\bar{U}$ are in much better agreement for $y/R > 0.07$ than the data scaled by u_τ. The only profile that is not in

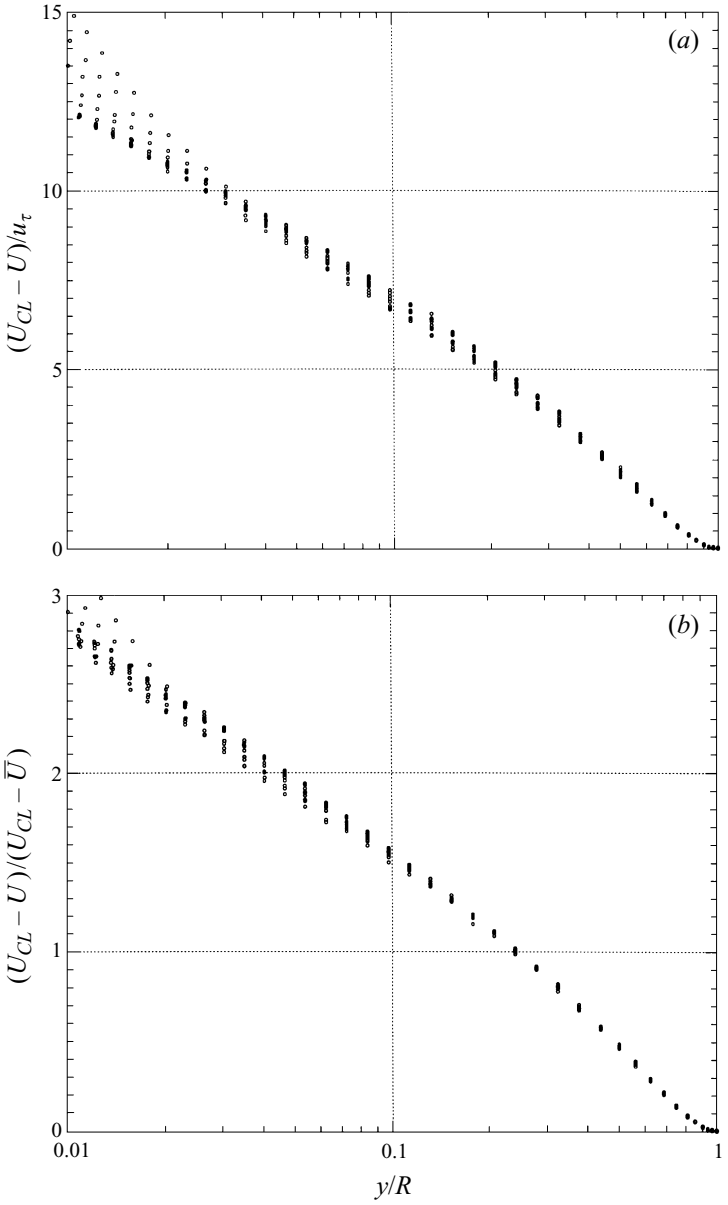

FIGURE 24. A comparison between the velocity profiles normalized by (*a*) u_τ and (*b*) $U_{CL}-\bar{U}$ for Reynolds numbers between 31×10^3 and 540×10^3.

good agreement with the others is that at the lowest Reynolds number, 31×10^3, which may indicate that the data near $y/R\approx0.1$ ($y^+\approx100$) scales on inner layer variables. This is consistent with our observation that the outer limit of the power law extends to $y\approx0.15R$ at low Reynolds numbers. For Reynolds numbers between 31×10^3 and 540×10^3, it appears that $U_{CL}-\bar{U}$ is a better outer velocity scale than u_τ.

To extend our comparison to Reynolds numbers lower than we investigated, we use the data measured by Toonder & Nieuwstadt (1997). In figure 25(*a*, *b*) their velocity profiles are shown normalized by u_τ and $U_{CL}-\bar{U}$, respectively, for four Reynolds numbers between 4.9×10^3 and 25×10^3. The collapse is poor for all Reynolds numbers

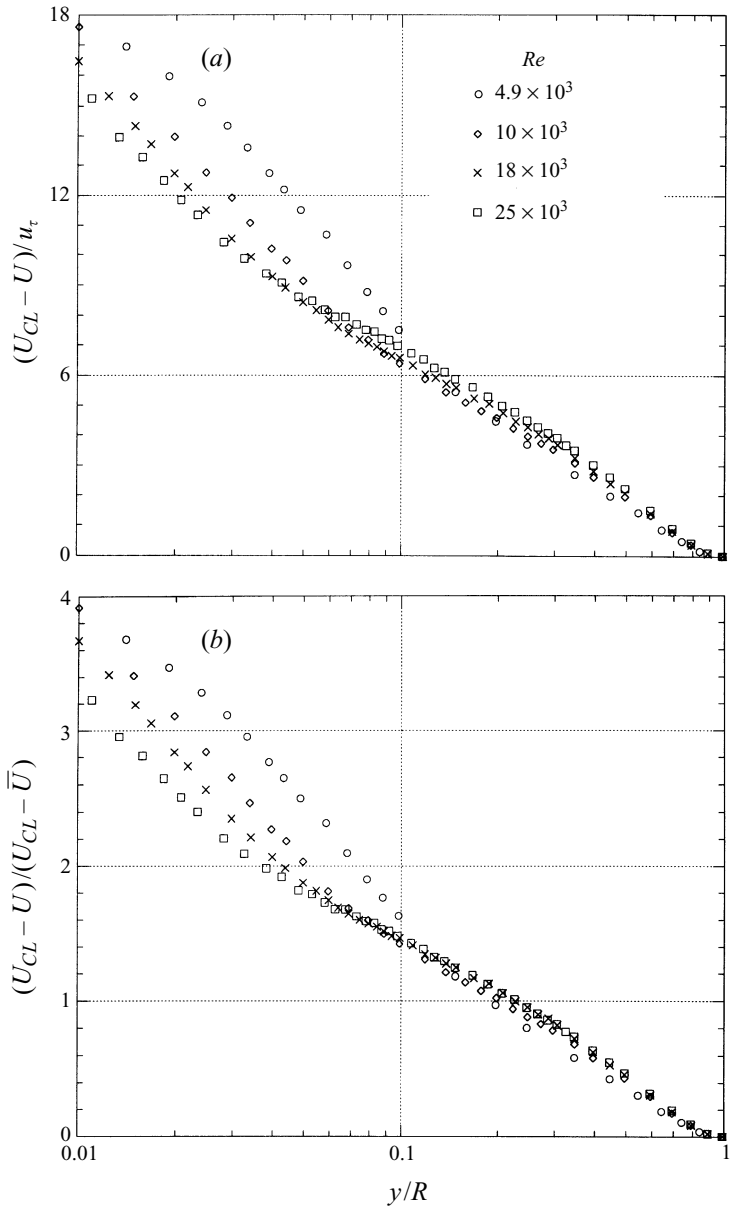

FIGURE 25. A comparison between the velocity profiles normalized by (*a*) u_τ and (*b*) $U_{CL}-\bar{U}$ for Reynolds numbers between 4.9×10^3 and 25×10^3. The data are from Toonder & Nieuwstadt (1997).

when normalized by u_τ. When normalized by $U_{CL}-\bar{U}$, the collapse is excellent for the two highest Reynolds numbers, $Re = 18\times10^3$ and 25×10^3, but it is less good for the two lowest Reynolds numbers, $Re = 4.9\times10^3$ and 10×10^3. This behaviour is expected because our analysis of the near-wall region indicates that an overlap region, a power law here, does not exist until $Re > 13\times10^3$, so we may expect that complete similarity does not exist in the near-wall and core regions until this Reynolds number is exceeded.

Toonder & Nieuwstadt also measured turbulence quantities which may be used to further evaluate the proposed outer velocity scale. The large-scale streamwise motions

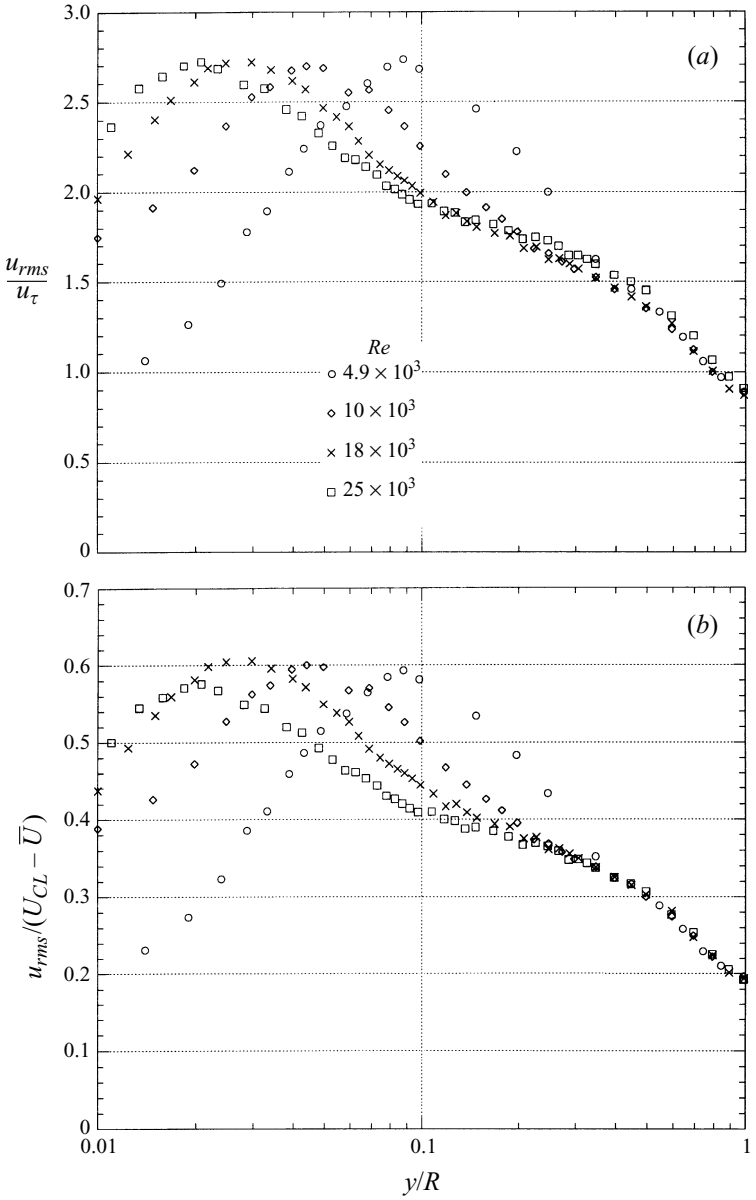

FIGURE 26. A comparison between the u_{rms} profiles normalized by (*a*) u_τ and (*b*) $U_{CL}-\bar{U}$ for Reynolds numbers between 4.9×10^3 and 25×10^3. The data are from Toonder & Nieuwstadt (1997).

should depend on the same outer velocity scale as the mean velocity profile. Since these motions contain most of the energy, we may expect that the root-mean-squared fluctuating velocity u_{rms} scales on outer layer variables in the core region (see Perry & Abell 1975, for example). In figure 26(*a*, *b*) the u_{rms} profiles are shown normalized by u_τ and $U_{CL}-\bar{U}$. The collapse is poor for all Reynolds numbers when normalized by u_τ. When normalized by $U_{CL}-\bar{U}$, the collapse is much improved for $0.2 < y/R < 1$ for the three highest Reynolds numbers, and for $0.4 < y/R < 1$ for the lowest Reynolds number. Note the improved collapse near the centreline when normalized by $U_{CL}-\bar{U}$.

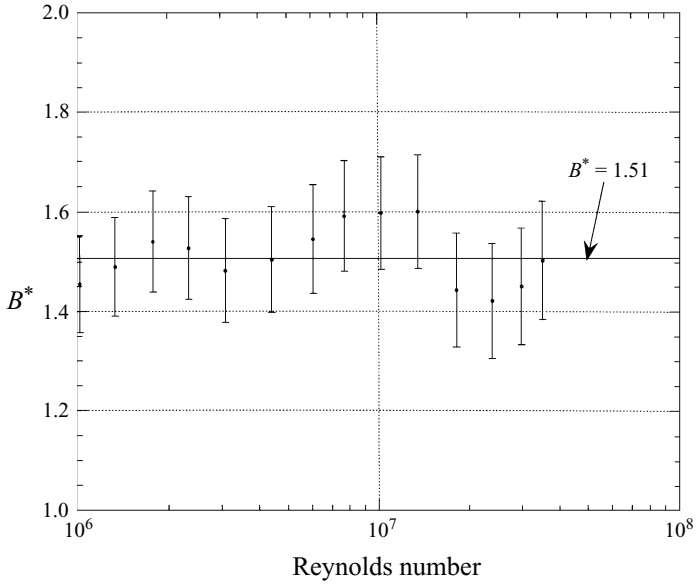

FIGURE 27. A plot showing the variation of B^* with Reynolds number.

This comparison may be more persuasive support of the proposed outer velocity scale than the comparisons using the mean velocity profiles. For the mean velocity profiles, the collapse near the centreline is insensitive to the choice of velocity scale since the velocity defect approaches zero at this point independent of our choice of velocity scale.

10. A new scaling argument for the outer region

At high Reynolds number, a log law should be apparent when the profiles are scaled by outer layer variables. To determine the additive constant in the log law, B^*, we assumed that $\kappa = 0.436$ which was shown to be consistent with the friction factor and centreline velocity data (§6), and velocity profiles when scaled by inner layer variables (§7). Next, for each Reynolds number, B^* was calculated for each data point in the logarithmic region which was shown to exist for $600/R^+ < y/R < 0.07$ (§7). The data points near the wall ($y/R < 0.01$) were neglected due to the relatively large uncertainty in their positions, and only Reynolds numbers with at least six data points in the assumed logarithmic region were analysed. At the higher Reynolds numbers, 15 data points were in the assumed log region.

The values of B^* at each Reynolds number were averaged (no-weighting) and the results are shown in figure 27. Also shown is an estimate for the uncertainty in B^* which is nominally ± 0.11. B^* has an approximately constant value of 1.51 with a standard error of 0.03 (95% confidence interval) for Reynolds numbers greater than 750×10^3. A similar analysis was performed using $U_{CL} - \bar{U}$ as the velocity scale. The additive constant becomes B^*/A which has a value of 0.348 ± 0.004, and the slope becomes $1/\kappa A$ which has a value of $1/(1.89 \pm 0.01)$.

For regions between $600/R^+ < y/R < 0.07$, a logarithmic overlap appears to exist which can be accurately represented by

$$\frac{U_{CL} - U}{U_{CL} - \bar{U}} = \frac{1}{1.89} \ln \eta + 0.348 \tag{55}$$

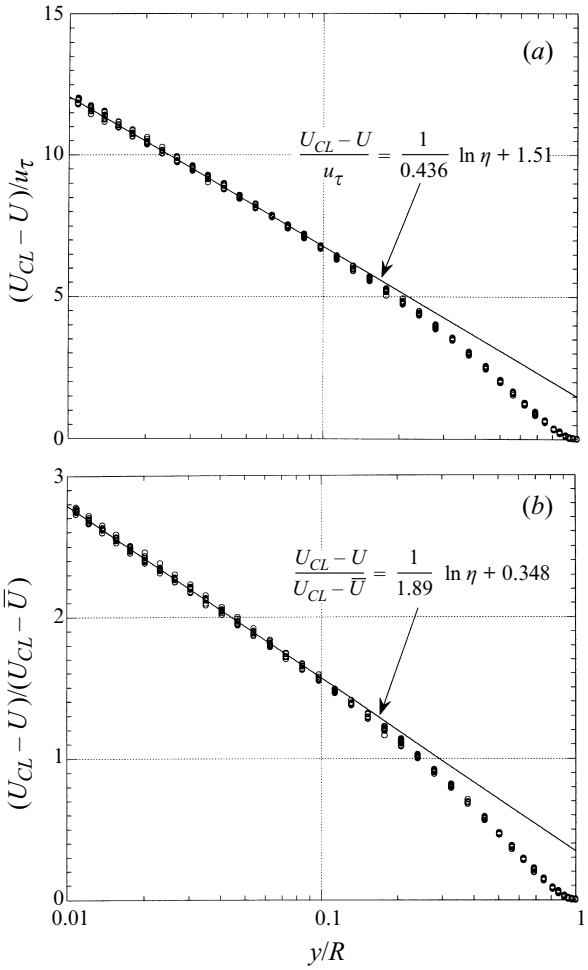

FIGURE 28. A comparison between the velocity profiles normalized by (*a*) u_τ and (*b*) $U_{CL}-\bar{U}$ for Reynolds numbers between 3.1×10^6 and 35×10^6.

or
$$\frac{U_{CL}-U}{u_\tau} = \frac{1}{0.436}\ln\eta + 1.51. \tag{56}$$

The velocity profile data are within $\pm1.5\%$ (95% confidence interval) of (55) and (56). The relatively large uncertainty can be attributed to the uncertainty in $U_{CL}-U$ which is the difference between two large numbers and consequently has a large uncertainty.

In figure 28(*a*, *b*) equations (56) and (55) are compared with the velocity profile data for Reynolds numbers between 3.1×10^6 and 35×10^6. For this range of Reynolds numbers, a log law should exist all the way to $y/R = 0.01$ since at the lowest Reynolds shown ($R^+ = 55\times10^3$), the inner limit of the log law is at $y^+/R^+ = 600/55\times10^3 \approx 0.01$, the origin for y/R. In figure 29(*a*) the velocity profiles are scaled by u_τ and in figure 28(*b*) they are scaled by $U_{CL}-\bar{U}$. The outer limit of the log law is approximately $y/R \approx 0.07$ in both figures which is consistent with our findings in §7. The agreement between the log law with the appropriate constants and the data is equally good for both figures, and it appears that at high Reynolds numbers the outer velocity scales are equivalent.

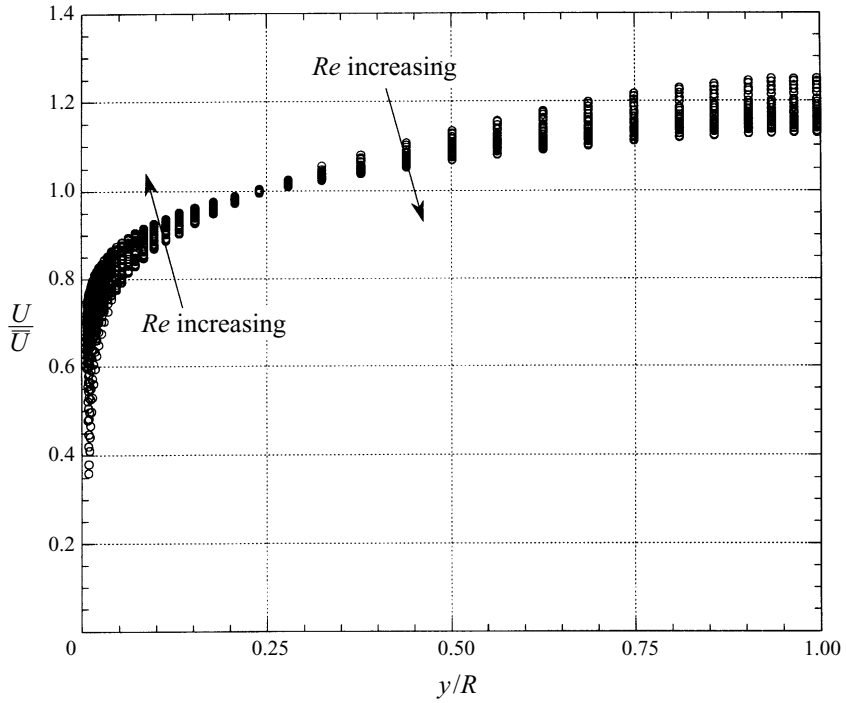

FIGURE 29. A plot showing the velocity profiles normalized by the average velocity for 26 different Reynolds numbers between 31×10^3 and 35×10^6.

We have proposed a new velocity scale for the outer region which appears to better collapse the velocity profile data than the scale proposed by von Kármán. The new outer scale is consistent with the scaling in the overlap and core regions. To further support our claim, in figure 29 we show the mean velocity profiles normalized by the average velocity for all 26 Reynolds numbers. The point where the velocity equals the average velocity is independent of Reynolds number and occurs at a location where $y_0 \approx 0.25R$ or $\eta_0 \approx 0.25$. From our analysis this point is located in the outer region where the scaling given by (48) should hold. At the point where $U = \bar{U}$, (48) gives

$$\frac{U_{CL} - \bar{U}}{U_{CL} - \bar{U}} = 1 = g(\eta_0) \tag{57}$$

and η_0 must be independent of Reynolds number. Figure 29 provides additional support for the proposed outer scaling. The new outer velocity scale can be linked to the well-documented 1/4-radius point that had been thought to lie in the log region (see Tennekes & Lumley 1972). It would appear that a one-point measurement is all that is required to accurately determine the average velocity in a fully developed smooth pipe flow for over three orders of magnitude in Reynolds numbers ($13 \times 10^3 < Re < 35 \times 10^6$).

It seems logical to extend this scaling argument to boundary layers. The outer velocity scale, $U_{CL} - \bar{U}$, is proportional to the mass flux deficit in the pipe. For a boundary layer, an equivalent outer velocity scale is given by

$$u_o = U_e - \bar{U} = U_e \int_0^1 \left(1 - \frac{U}{U_e}\right) \mathrm{d}\left(\frac{y}{\delta}\right) = U_e \frac{\delta^*}{\delta}, \tag{58}$$

where U_e is the velocity at the edge of the boundary layer, δ^* is the displacement

thickness and δ is the boundary layer thickness. A noteworthy feature of this new scale is that it can be accurately determined from the velocity profiles, in contrast to u_τ which is not easily measured in a boundary layer. At high Reynolds numbers, we can expect that $\delta^*/\delta \sim C_f^{1/2}$, where C_f is the skin friction coefficient given by

$$C_f = 2(u_\tau/U_e)^2, \tag{59}$$

for a logarithmic overlap region to exist. A comparison of this theory with experimental boundary layer data is left for future work, but in the light of our success for pipe flow, we believe that this scale is the correct scale for the outer region of boundary layers, and we are currently preparing a comparison with data.

11. Conclusions

An experimental investigation was conducted to determine the mean-flow scaling in a fully developed, smooth pipe flow. A new friction factor relation was proposed which is similar to Prandtl's, but has different constants and includes an additional term to account for the near-wall velocity profile. This new relation accurately represents the subtleties of the mean velocity profiles.

At small values of R^+, but which are large enough that an overlap region exists, the mean velocity profile in the overlap region is given by a power law. The power law exists in a discrete region between the inner region and outer region or logarithmic overlap region, depending on the magnitude of the Reynolds number, and the empirical constants in the power law do not depend on Reynolds number when expressed using inner scaling variables. We argue that this region is not the overlap region expected at very large Reynolds number, but an intermediate overlap region that covers the range of y^+ at which most previous experiments have been performed. At very large Reynolds number, another overlap region is apparent, and the scaling in this region appears to be logarithmic. The log law is only evident if the pipe Reynolds number is greater than approximately 400×10^3.

A new theory was developed to explain the scaling in both overlap regions. This theory requires a velocity scale for the outer region such that the ratio of the outer velocity scale to the inner velocity scale (the friction velocity) is a function of Reynolds number at low Reynolds numbers, and approaches a constant value at high Reynolds numbers. The proposed velocity scale was used to normalize the velocity profiles in the outer region and was found to give significantly better agreement between different Reynolds numbers than the friction velocity. The proposed velocity scale was also used to normalize the u_{rms} profiles measured by Toonder & Nieuwstadt (1997) and was found to give significantly better agreement between different Reynolds numbers than the friction velocity.

The new outer velocity scale presented here was established for a pipe flow. For similar values of R^+, we may expect channel flow and boundary layers to scale the same way as pipe flow. An equivalent outer velocity scale for a boundary layer is given by $u_o = U_e\delta^*/\delta$. At high Reynolds numbers, δ^*/δ should be proportional to $C_f^{1/2}$ for a logarithmic overlap region to exist.

Discussions with V. Yakhot, S. A. Orszag, A. E. Perry, D. Coles and P. Bradshaw were very helpful in preparing this manuscript. The support of ARPA/ONR under Grant N00014-92-J-1796 is gratefully acknowledged.

REFERENCES

Abell, C. J. 1974 Scaling laws for pipe flow turbulence. Doctoral Dissertation, University of Melbourne.

Afzal, N. & Yajnik, J. 1973 *J. Fluid Mech.* **61**, 23.

Barenblatt, G. I. 1993 *J. Fluid Mech.* **248**, 513.

Blasius, H. 1913 *Forschg. Arb. Ing.* 131.

Brederode, V. de & Bradshaw, P. 1974 *IC Aero. Rep.* 74-03. Imperial College of Science and Technology, Dept. of Aeronautics.

Chue, S. H. 1975 *Prog. Aerospace Sci.* **16**, 147.

Clauser, F. H. 1956 *Adv. Appl. Mech.* **4**, 1.

Coles, D. E. 1955 In *Tollmien & Görtler; Fifty Years of Boundary Layer Research*. Vieweg.

Davies, P. O. A. L. 1958 *J. Fluid Mech.* **3**, 441.

Dean, R. B. & Bradshaw, P. 1976 *J. Fluid Mech.* **78**, 641.

Deissler, R. G. 1950 *NACA Tech. Note* 2138.

Dickinson, J. 1975 Turbulent skin friction techniques. Internal Report, Laval University, Quebec.

Durand, W. F. 1943 *Aerodynamic Theory*, Vol. 3. California Institute of Technology.

George, W. K., Castillo, L. & Knecht, P. 1996 *Tech. Rep.* TRL-153. SUNY at Buffalo.

George, W. K., Castillo, L. & Wosnik, M. 1997 *Theoretical and Applied Mechanics Rep.* 872. University of Illinois at Urbana-Champaign.

Hama, F. R. 1954 *Trans. SNAME* **62**, 333.

Hinze, J. O. 1964 In *Intl Symp. of the National Scientific Research Center*. Gordon and Breach.

Holman, J. P. 1989 *Experimental Methods for Engineers*. McGraw-Hill.

Ito, H. 1959 *Trans. ASME*: *J. Basic Engng* **6**, 123.

Kármán, T. von 1930 *Nacht. Ges. Wiss. Goett. Math.-Phys. Kl.*, 58.

Laufer, J. 1954 *NACA Rep.* 1174.

Livesey, H. J. L. 1956 *J. Aeronaut. Sci.* **23**, 949.

Long, R. R. 1979 *Tech. Rep.* 16 (C). The Johns Hopkins University.

MacMillan, F. A. 1956 *Ministry of Supply*, *Aero. Res. Counc. R. & M.* 3028.

McDonald, A. T. & Fox, R. W. 1966 *Intl J. Mech. Sci.* **8**, 125.

Mehta, R. D. & Bradshaw, P. 1979 *Aero. J.* 718.

Millikan, C. M. 1938 In *Proc. 5th Intl Congr. Appl. Mech.* Wiley.

Muzas, B. 1995 Absolute distance measurement by means of electrical capacitance in the ARPA/Princeton SuperPipe. Undergraduate Independent Project, Department of Mechanical and Aerospace Engineering, Princeton University.

Nikuradse, J. 1930 *Ing.-Arch.* **1**, 306.

Nikuradse, J. 1932 *Forsch. Arb. Ing.-Wes.* no. 356 (English transl. *NACA TT* F-10, 359).

Nikuradse, J. 1933 *Forsch. Arb. Ing.-Wes.* no. 361 (English transl. *NACA TM* 1292).

Ozarapoglu, V. 1972 Measurements in incompressible turbulent flows. Doctoral Thesis, University of Laval.

Patel, V. C. 1965 *J. Fluid Mech.* **23**, 185.

Patel, V. C. & Head, M. R. 1969 *J. Fluid Mech.* **38**, 181.

Perry, A. E. & Abell, C. J. 1975 *J. Fluid Mech.* **67**, 257.

Prandtl, L. 1933 *Z. Ver. Dtsch. Ing.* **77**, 105 (English transl. *NACA TM* 720).

Schlichting, H. 1987 *Boundary-Layer Theory*. McGraw-Hill.

Shaw, R. 1960 *J. Fluid Mech.* **7**, 550.

Spalding, D. B. 1961 *J. Appl. Mech.* **28**, 455.

Stanton, T. E. 1911 *Proc. R. Soc. Lond.* A **85**, 366.

Tennekes, H. 1968 *AIAA J.* **6**, 1735.

Tennekes, H. & Lumley, J. L. 1972 *A First Course in Turbulence*. MIT Press.

Toonder, J. M. J. den & Nieuwstadt, F. T. M. 1997 *Phys. Fluids* **9**, 3398.

Townes, H. W., Gow, J. L., Powe, R. E. & Weber, N. 1972 *Trans. ASME J. Basic Engng* **6**, 353.

Zagarola, M. V. 1996 Mean-flow scaling of turbulent pipe flow. Doctoral Dissertation, Princeton University.

Zagarola, M. V., Perry, A. E. & Smits, A. J. 1997 *Phys. Fluids* **9**, 2094.

Zagarola, M. V. & Smits, A. J. 1997 *Phys. Rev. Lett.* **78**, 239.

Zagarola, M. V., Smits, A. J., Orszag, S. A. & Yakhot, V. 1996 *AIAA Paper* 96-0654.